~~CONFIDENTIAL~~

Copy
RM L54C26

NACA RM L54C26

NACA

RESEARCH MEMORANDUM

WIND-TUNNEL INVESTIGATION OF EFFECT OF SWEEP ON ROLLING DERIVATIVES AT ANGLES OF ATTACK UP TO 13° AND AT HIGH SUBSONIC MACH NUMBERS, INCLUDING A SEMIEMPIRICAL METHOD OF ESTIMATING THE ROLLING DERIVATIVES

By James W. Wiggins

Langley Aeronautical Laboratory
Langley Field, Va.

THIS DOCUMENT AND EACH AND EVERY PAGE HEREIN IS HEREBY RECLASSIFIED FROM Conf TO Unclass AS PER LETTER DATED Per Auth Ltr # 113 OSI

ENGINEERING DEPT. LIBRARY
CHANCE-VOUGHT AIRCRAFT
DALLAS, TEXAS

CLASSIFIED DOCUMENT

This material contains information affecting the National Defense of the United States within the meaning of the espionage laws, Title 18, U.S.C., Secs. 793 and 794, the transmission or revelation of which in any manner to an unauthorized person is prohibited by law.

NATIONAL ADVISORY COMMITTEE
FOR AERONAUTICS

WASHINGTON
April 27, 1954

~~CONFIDENTIAL~~

NATIONAL ADVISORY COMMITTEE FOR AERONAUTICS

RESEARCH MEMORANDUM

WIND-TUNNEL INVESTIGATION OF EFFECT OF SWEEP ON ROLLING DERIVATIVES AT ANGLES OF ATTACK UP TO 13° AND AT HIGH SUBSONIC MACH NUMBERS, INCLUDING A SEMIEMPIRICAL METHOD OF ESTIMATING THE ROLLING DERIVATIVES

By James W. Wiggins

SUMMARY

An investigation was performed in the Langley high-speed 7- by 10-foot wind tunnel in order to determine the rolling derivatives for swept-wing--body configurations at angles of attack from 0° to 13° and at high subsonic Mach numbers. The wings had sweep angles at the quarter-chord line of 3.6°, 32.6°, 45°, and 60°, an aspect ratio of 4, a taper ratio of 0.6, and an NACA 65A006 airfoil section parallel to the free stream. The results indicate a reduction in the damping-in-roll derivative C_{l_p} at the higher test angles of attack. Of the wings tested, instability of the damping-in-roll derivative C_{l_p} was experienced over the largest ranges of angle of attack and Mach number for the 32.6° swept-back wing.

In general, the variation of the damping-in-roll derivative C_{l_p} with sweep angle at zero angle of attack was only in fair agreement with the predicted variation, inasmuch as the 32.6° sweptback wing showed more damping C_{l_p} at zero angle of attack in the Mach number range from 0.85 to 0.93 than any of the other plan forms. The predicted variation of C_{l_p} at zero angle of attack with Mach number was in good agreement with the experimental trend up to the critical Mach number. Contrary to predictions based on potential-flow theory, the yawing moment due to rolling C_{n_p} was positive and the lateral force due to rolling C_{Y_p} was negative at the higher test angles of attack throughout the test range of Mach number for all configurations. Presented herein is a method of estimating yawing moment due to rolling C_{n_p} and lateral force due to rolling C_{Y_p} through the test-angle-of-attack range. The method is shown to be applicable over large ranges of leading-edge radii, wing thickness, and Mach number. The results indicate a loss of wing-tip suction within the ranges of Mach number and angle of attack investigated.

CONFIDENTIAL

ENGINEERING DEPT. LIBRARY
CHANCE-VOUGHT AIRCRAFT
DALLAS, TEXAS

INTRODUCTION

The present investigation is a continuation of a program being conducted in the Langley high-speed 7- by 10-foot tunnel in order to determine the effects of wing geometry and angle of attack on rolling stability derivatives at high subsonic speeds. Reported herein are results on the effect of sweep angle and angle of attack on the rolling derivatives for a body in combination with various wings. The wings tested had sweep angles of 3.6°, 32.6°, 45°, and 60° at the quarter-chord line and had a taper ratio of 0.6, an aspect ratio of 4, and an NACA 65A006 airfoil section parallel to the free stream. Tests were also conducted on the 45° sweptback wing with wing fences located at the 65-percent-semispan station, since an appreciable loss of damping in roll C_{l_p} was noted at the higher test angles of attack for the clean-wing configuration.

The longitudinal and lateral stability characteristics of the wing-body and body-alone configurations are presented in references 1 to 3. The wing geometry is designated as in reference 2. For example, the designation 3.6-4-.6-006 denotes a wing with the quarter-chord line swept back 3.6° with an aspect ratio of 4, a taper ratio of 0.6, and a 6-percent-thick airfoil section with zero camber.

COEFFICIENTS AND SYMBOLS

The stability system of axes used for the presentation of the results, together with an indication of the positive forces, moments, velocities, and angles, is presented in figure 1. All moments are referred to the projection of the quarter-chord point of the wing mean aerodynamic chord on the fuselage center line.

C_l rolling-moment coefficient, $\frac{\text{Rolling moment}}{qSb}$

C_n yawing-moment coefficient, $\frac{\text{Yawing moment}}{qSb}$

C_Y lateral-force coefficient, $\frac{\text{Lateral force}}{qS}$

C_D drag coefficient, Drag/qS

C_L lift coefficient, Lift/qS

q dynamic pressure, $\rho V^2/2$, lb/sq ft

ρ mass density of air, slugs/cu ft

p rate of roll, radians/sec

Λ sweep angle at quarter-chord line, deg

V free-stream velocity, ft/sec

M Mach number

R Reynolds number

S wing area, sq ft

b wing span, ft

c wing chord, ft

$\bar{c}$ mean aerodynamic chord, ft

l body length

d body diameter

A aspect ratio, b^2/S

α angle of attack, deg

$\frac{pb}{2V}$ wing-tip helix angle, radians

$$C_{l_p} = \frac{\partial C_l}{\partial \frac{pb}{2V}} \text{ per radian}$$

$$C_{n_p} = \frac{\partial C_n}{\partial \frac{pb}{2V}} \text{ per radian}$$

$$C_{Y_p} = \frac{\partial C_Y}{\partial \frac{pb}{2V}} \text{ per radian}$$

[redacted]

MODEL AND APPARATUS

A sketch of the models investigated and details of the fence are shown in figure 2. All wings except the 45° swept wing were constructed of 24S-T aluminum alloy. The 45° swept wing had a steel core with a bismuth-tin covering. The wings had a taper ratio of 0.6, an aspect ratio of 4, and an NACA 65A006 airfoil section and were attached to the fuselage in a midwing position. The geometric characteristics of the body are presented in table I.

The models were tested on the forced-roll sting-support system shown in figure 3. Details of the operation of the roll sting and the technique of recording the data are discussed in reference 4. Angles of attack were obtained by means of offset sting adapters in the sting behind the model (fig. 3). The forces and moments were measured on an internally mounted electrical strain-gage balance.

TESTS AND CORRECTIONS

The forced-roll tests were made in the Langley high-speed 7- by 10-foot tunnel through a Mach number range from 0.50 to 0.95 and through a maximum angle-of-attack range from 0° to 13°. Tests were also conducted on the 45° swept wing with wing fences located at the 65-percent-semispan station. The variation with Mach number of the mean test Reynolds number (based on the mean aerodynamic chord of the wing) and the maximum test values of $pb/2V$ are presented in figures 4 and 5, respectively.

The blocking corrections applied to the dynamic pressure and Mach number were determined by the velocity-ratio method of reference 5. Drag and angle of attack were corrected for jet-boundary effects by the method of reference 6, but an investigation of the jet-boundary corrections to the rolling derivatives by methods similar to those used in reference 7 indicated that these corrections were negligible. Tare tests were made at zero angle of attack with and without a simulated offset sting adapter behind a similar model and the effects were found to be negligible.

The data presented have been corrected for inertia forces and moments that were introduced as the model was rotated, with consideration being given to deflections of the entire support system under aerodynamic loads.

In order to evaluate the aeroelastic corrections to C_{l_p} at zero angle of attack, the wings were statically loaded in accordance with theoretical load distributions obtained from reference 8. The resulting incremental changes in wing-section angle of attack have been interpreted

in terms of equivalent rotational velocities and the results are presented in figure 6. Values of the equivalent linear twist distribution indicated at $\frac{Y}{b/2} = 1.0$ can be interpreted as correction increments

$$\frac{\Delta\left(\frac{pb}{2V}\right)}{qC_l}$$

which can be applied to the measured values of $pb/2V$ according to the equation

$$C_{l_p} = \frac{(C_l)_{meas}}{\frac{pb}{2V} - \Delta\frac{pb}{2V}} = \frac{\left(C_{l_p}\right)_{meas}}{1 - \frac{\Delta(pb/2V)q}{qC_l}\left(\frac{C_l}{pb/2V}\right)_{meas}}$$

or

$$C_{l_p} = \frac{\left(C_{l_p}\right)_{meas}}{1 - k\left(C_{l_p}\right)_{meas}}$$

where

$$k = \frac{\Delta(pb/2V)q}{qC_l}$$

and is presented as a function of Mach number in figure 7.

Distortion effects on C_{n_p} and C_{Y_p} have been roughly estimated and, since these effects appeared to be small over the test angle-of-attack range for all wings, they have been neglected.

The angle of attack at the plane of symmetry has been corrected for the deflection of the model and support system under load. All data are referred to the stability axes system.

[redacted]

RESULTS AND DISCUSSION

The results of the present investigation are presented as outlined in the following table:

Results	Figure
C_l against pb/2V	8
C_n against pb/2V	9
C_{l_p} against α	10
C_L against M (C_{l_p} boundaries)	11
C_{n_p} against α	12
C_{Y_p} against α	13
C_{l_p} against M (compared with calculations)	14
C_{l_p} against Λ (compared with calculations)	15
C_{l_p} against α (compared with calculations)	16
C_{Y_p} against α (compared with calculations)	17
C_D against α	18 and 19
C_{n_p} against α (compared with calculations)	20 to 22
C_{Y_p} against α (compared with calculations)	23 and 24

Results of C_l and C_n plotted against pb/2V are presented in figures 8 and 9 only for those angle-of-attack conditions for which pronounced nonlinearities, with respect to pb/2V, were indicated. For all conditions not covered in figures 8 and 9, the data were sufficiently linear to permit adequate representations of the results by means of derivatives with respect to pb/2V.

Experimental Rolling Derivatives

Rolling moment due to rolling.- In general, the damping due to roll C_{l_p} decreased above an angle of attack of about 6° (fig. 10), and in the region of low damping or positive values of C_{l_p}, the variation of rolling moment with rolling velocity was rather erratic (fig. 8). These nonlinearities and ranges of uncertainties of C_l against pb/2V are difficult to analyze in quantitative terms of C_{l_p} (see shaded areas

of figs. 10, 11, and 16, which are approximately average values of C_{l_p}) and, therefore, the application of the data with respect to controllability, rolling, and dynamic stability should be carefully considered. Some additional remarks on the damping for these wings are given in reference 9.

At an angle of attack of 11° and a Mach number of 0.85, the 3.6° swept-wing data (fig. 8(a)) show a pronounced hysteresis. The data were obtained by rolling the model from the extreme negative values of pb/2V to the extreme positive values of pb/2V, then back through the pb/2V range. It should be pointed out that these nonlinearities and hystereses occur above the angle of attack at which this wing indicates a peak in the lift curve (ref. 1).

The results for the 32.6° swept wing (figs. 8(b) and 10) show that, in general, at the higher Mach numbers and angles of attack, an unstable condition (positive values of C_{l_p}) is apparent over a wide range of rolling velocities; whereas a stable condition is indicated only at the extreme rates of roll. The results presented in figure 11 show that, of the wings investigated, the results for this plan form showed unfavorable damping-in-roll characteristics (indicated by C_{l_p}) over the largest test ranges of Mach number and angle of attack.

The 45° sweptback wing shows only a small region of zero or reverse damping - occurring at a Mach number of 0.91, an angle of attack of about 10.8°, and at low values of pb/2V. (See figs. 8 and 10.) Considerable loss in damping did exist, however, at the higher test angles of attack throughout the test range of Mach number. The configuration with fences installed did not exhibit as much loss of damping at higher angles of attack as did the clean configuration. As was shown in reference 10, the fences improve the lifting capabilities of the airfoil sections near the wing tips on the 45° swept wing and, therefore, improve the damping in roll as well as the high-lift longitudinal stability. (See refs. 9 and 11.)

The decrease in damping noted for all wings at the higher test angles of attack is probably associated with tip-stalling as shown for the 45° sweptback wing in references 10 and 12.

Yawing moment and lateral force due to rolling.- The variation of the yawing-moment-due-to-rolling derivative C_{n_p} with angle of attack is presented in figure 12. The general trend of C_{n_p} with angle of attack is similar for all wings; that is, zero or slightly negative values are obtained at the lower angles of attack and positive values are obtained at the higher test angles of attack.

[redacted]

In figure 13, the variation of C_{Y_p} with angle of attack is presented. Negative values of C_{Y_p} (lateral force due to rolling) are indicated at the higher test angles of attack and at most Mach numbers for all configurations tested. A discussion and possible explanation of the behavior of C_{n_p} and C_{Y_p} through the test angle-of-attack and Mach number range and a method for estimating these derivatives are presented in the following section.

Estimations of Rolling Derivatives

Rolling moment due to rolling.- A comparison of the experimental and calculated variations of C_{l_p} at zero angle of attack with Mach number is presented in figure 14. The calculated variations were evaluated by the methods described in references 8 and 13. The predicted trend, at least up to the critical Mach number, is in fairly good agreement with experiment. The aeroelastic effects are seen to be of appreciable magnitude for the 45° and 60° sweptback wings.

The variation of C_{l_p} at zero angle of attack with sweep angle presented in figure 15 shows that, at the higher Mach numbers (0.85 to 0.93), the 32.6° sweptback wing has higher values of damping, corrected for aeroelasticity, than the other test wings, although the calculations of references 8 and 13 predict a decrease in C_{l_p} with increasing sweep angle.

A comparison of the variation of C_{l_p} with angle of attack, for all configurations tested, determined by experiment and calculations, is shown in figure 16. Values of C_{l_p} at zero angle of attack were determined from reference 8, and compressibility effects were evaluated from reference 13. Angle-of-attack effects were determined by the procedure of reference 14 using experimental lift-curve slopes of references 1 and 2. It has been shown in reference 15 that root-bending-moment data would be more appropriate than lift data in evaluating angle-of-attack effects on C_{l_p}; however, bending-moment data were not available at these angles of attack for the wings of the present investigation. The quantitative agreement shown in figure 16 is not very good; however, the experimental and predicted values show similar trends.

Yawing moment due to rolling.- In references 15 and 16, methods are presented for the prediction of C_{n_p} through an angle-of-attack range using corresponding experimental drag data. The method in reference 15 has been shown to predict C_{n_p} through the test angle-of-attack range

with considerably better results than the method described in reference 16. This result is probably due to the fact that the method of reference 16 predicts C_{n_p} by extrapolating from the potential-flow theory by use of experimental drag data and an empirically determined factor that is proportional to a drag-center moment arm; whereas the procedure of reference 15 predicts C_{n_p} by using the experimental drag data to proportion C_{n_p} relative to two known conditions. Briefly, the method of reference 15 consists of proportioning C_{n_p} relative to the condition of potential flow where the resultant force is normal to the relative wind and to the condition for which the resultant force is normal to the wing chord. An equation is presented therein for evaluating C_{n_p} for triangular wings. However, for other wing plan forms, this equation must be modified as follows: the potential-flow value of C_{n_p} for triangular plan forms (ref. 17) must be replaced by the value for wings of taper ratios other than 0, and an additional term, shown in reference 16 for low-aspect-ratio wings to be a result of wing-tip suction, must be considered. With these considerations applied, the following equation can be written:

$$C_{n_p} = -C_{l_p} \tan \alpha - K\left(-C_{l_p} \tan \alpha - \frac{C_{n_p}}{C_L} C_L\right) + \left(C_{n_p}\right)_{\text{tip suction}} \qquad (1)$$

where the potential-flow values of C_{n_p}/C_L can be determined from reference 18 and either experimental or calculated values of C_{l_p} can be used. The factor K is a dimensionless factor that relates C_{n_p} to any intermediate flow condition that exists between the conditions where the resultant force is normal to the relative wind and where the resultant force is normal to the wing chord and can be determined from the drag data of figures 18 and 19 as follows:

$$K = \frac{\frac{\partial}{\partial \alpha}(C_L \tan \alpha) - \frac{\partial}{\partial \alpha}\left(C_D - C_{D_{C_L}} = 0\right)_{\text{exp}}}{\frac{\partial}{\partial \alpha}(C_L \tan \alpha) - \frac{\partial}{\partial \alpha} \frac{C_L^2}{\pi A}}$$

The tip-suction contribution is expressed in reference 16 as

$$\left(C_{n_p}\right)_{\text{tip suction}} = \left(-C_{Y_p}\right)_{\Lambda=0^\circ} \frac{d}{b}$$

[redacted]

where d is the longitudinal distance from the midchord point at the wing tip to the coordinate origin and is defined as

$$d = \frac{b}{2(1 + \lambda)}\left(\frac{2 + \lambda}{3}\tan \Lambda + \frac{\lambda}{A}\right) + X'$$

where X' is the longitudinal distance rearward from the coordinate origin to the wing aerodynamic center. An attempt was made in reference 16 to account for tip suction by correlating data obtained at low speeds on 12-percent-thick unswept wings with the slender-triangular-body theory of reference 17. Shown in reference 16 is an empirical expression, determined from a limited amount of data, that expresses the tip-suction contribution as

$$\left(C_{Y_p}\right)_{\Lambda=0^\circ} = \frac{C_L}{A}$$

The tip-suction contribution to C_{n_p} can be written now in terms of the empirically determined suction force and moment arm as

$$\left(C_{n_p}\right)_{\text{tip suction}} = -\frac{C_L}{2A(1 + \lambda)}\left(\frac{2 + \lambda}{3}\tan \Lambda + \frac{\lambda}{A}\right) - \frac{C_L}{A}\frac{X'}{b}$$

For the wings of the present investigation, X' is equal to 0. The results presented in figure 20 at a Mach number of 0.70 show that values of C_{n_p} evaluated by use of equation (1), using calculated values of C_{l_p}, are in better agreement with experiment than values determined independently of the consideration of tip suction by the method of reference 16. It should be pointed out, although not shown, that a similar comparison of the two methods was obtained for the other wings tested. Better agreement is indicated when the tip suction in equation (1) is assumed to be 0; however, this result is not surprising inasmuch as the experimental values of C_{Y_p} for the unswept wing (which are due primarily to tip suction) presented in figure 17 indicate that, within the test ranges of Mach number and angle of attack, the tip-suction contribution can be neglected. The data for a Mach number of 0.15 (fig. 17) were obtained from reference 19.

The leading-edge contribution to C_{n_p} would be expected to vary considerably with leading-edge radii; consequently, in figure 21 low-speed

results are presented for 12-percent-thick wings (ref. 20) whose leading-edge radii vary from a very sharp one to a very blunt one. The wings reported in reference 20 had an aspect ratio of 2.61, a taper ratio of 1.0, and 45° sweepback. A comparison of experimental C_{n_p} with calculated values evaluated by use of equation (1) is presented in figure 22 for the wings of the present investigation at various Mach numbers where both experimental and calculated values of C_{l_p} were used; the tip-suction contribution to C_{n_p} was assumed to be 0. The agreement is considered good for all wings tested where either experimental or calculated C_{l_p} are used in equation (1), and the results presented in figures 21 and 22 indicate that the present method of estimating C_{n_p} (eq. (1)), without tip-suction effects, is applicable over large ranges of leading-edge radii, wing thickness, and subsonic Mach numbers.

Lateral force due to rolling.- An expression for determining C_{Y_p} for the potential-flow case can be obtained from reference 18 and written as

$$C_{Y_p} = C_L\left(\frac{A + \cos\Lambda}{A + 4\cos\Lambda}\tan\Lambda\right)$$

and, for the nonpotential case, when the resultant force is normal to the wing chord plane, C_{Y_p} would be equal to 0. By considering the tip-suction contribution and by applying the factor K, the equation can be written

$$C_{Y_p} = K\left(C_L\frac{A + \cos\Lambda}{A + 4\cos\Lambda}\tan\Lambda\right) + \left(C_{Y_p}\right)_{\text{tip suction}} \qquad (2)$$

where the tip contribution to C_{Y_p} can be expressed as

$$\left(C_{Y_p}\right)_{\text{tip suction}} = \frac{C_L}{A}$$

In figure 23, values of C_{Y_p} evaluated by equation (2) and values determined by the potential-flow methods of references 16 and 18 are compared with low-speed data of reference 20. In the application of equation (2), the contribution of the tip was assumed to be zero; however, the order of magnitude of the tip-suction contribution is indicated

[redacted]

in the comparison of the values determined by the procedures described in references 16 and 18. Better agreement is indicated when equation (2) of the present paper is used; however, this agreement is not surprising inasmuch as the methods of references 16 and 18 do not account for any nonpotential-flow effects on the leading-edge contribution. The results of the present investigation are compared with values evaluated by use of equation (2), without tip-suction effects, in figure 24. The agreement shown is reasonably good, particularly the negative trend indicated at the higher test angles of attack.

CONCLUSIONS

An investigation conducted to determine the effects of sweep angle on the rolling derivatives at high subsonic Mach numbers and high angles of attack for a series of swept wings of aspect ratio 4, taper ratio of 0.6, and having NACA 65A006 airfoil sections indicates the following conclusions:

1. The results show large reductions in the damping-in-roll derivative C_{l_p} at the higher test angles of attack for all wings tested. Of the wings investigated, the results for the 32.6° sweptback wing showed unfavorable damping-in-roll characteristics (indicated by C_{l_p}) over the largest ranges of angle of attack and Mach number.

2. Wing fences on the 45° sweptback wing at the 65-percent-semispan station are shown to improve the damping-in-roll derivative C_{l_p} at the higher test angles of attack relative to the clean-wing configuration.

3. In general, the variation of the damping-in-roll derivative C_{l_p} at zero angle of attack with sweep angle was only in fair agreement with the predicted variation with sweep angle, inasmuch as the 32.6° sweptback wing showed more damping in roll in the Mach number range from 0.85 to 0.93 than any of the other plan forms.

4. The predicted variation of C_{l_p} at zero angle of attack with Mach number was in good agreement with the experimental trend up to the critical Mach number.

5. Contrary to predictions based on potential-flow theory, the yawing moment due to rolling C_{n_p} was positive and the lateral force due to rolling C_{Y_p} was negative at the higher test angles of attack for all wings tested.

[redacted]

6. The results indicate a loss in wing-tip suction within the test ranges of Mach number and angle of attack investigated.

7. Presented herein is a method of estimating C_{n_p} (yawing moment due to rolling) and C_{Y_p} (lateral force due to rolling) through the test angle-of-attack range. This method is shown to be applicable over large ranges of leading-edge radii, wing thickness, and subsonic Mach numbers.

Langley Aeronautical Laboratory,
National Advisory Committee for Aeronautics,
Langley Field, Va., March 11, 1954.

[redacted]

REFERENCES

1. Wiggins, James W., and Kuhn, Richard E.: Wind-Tunnel Investigation of the Aerodynamic Characteristics in Pitch of Wing-Fuselage Combinations at High-Subsonic Speeds. Sweep Series. NACA RM L52D18, 1952.

2. Kuhn, Richard E., and Wiggins, James W.: Wind-Tunnel Investigation of the Aerodynamic Characteristics in Pitch of Wing-Fuselage Combinations at High Subsonic Speeds. Aspect-Ratio Series. NACA RM L52A29, 1952.

3. Kuhn, Richard E., and Fournier, Paul G.: Wind-Tunnel Investigation of the Static Lateral Stability Characteristics of Wing-Fuselage Combinations at High Subsonic Speeds - Sweep Series. NACA RM L52G11a, 1952.

4. Kuhn, Richard E., and Wiggins, James W.: Wind-Tunnel Investigation To Determine the Aerodynamic Characteristics in Steady Roll of a Model at High Subsonic Speeds. NACA RM L52K24, 1953.

5. Hensel, Rudolph W.: Rectangular-Wind-Tunnel Blocking Correction Using the Velocity-Ratio Method. NACA TN 2372, 1951.

6. Gillis, Clarence L., Polhamus, Edward C., and Gray, Joseph L., Jr.: Charts for Determining Jet-Boundary Corrections for Complete Models in 7- by 10-Foot Closed Rectangular Wind Tunnels. NACA WR L-123, 1945. (Formerly NACA ARR L5G31.)

7. Evans, J. M., and Fink, P. T.: Stability Derivatives. Determination of l_p by Free Oscillations. Rep. ACA-34, Australian Council for Aeronautics, Apr. 1947.

8. Bird, John D.: Some Theoretical Low-Speed Span Loading Characteristics of Swept Wings in Roll and Sideslip. NACA Rep. 969, 1950. (Supersedes NACA TN 1839.)

9. Kuhn, Richard E.: Notes on Damping in Roll and Load Distributions in Roll at High Angles of Attack and High Subsonic Speeds. NACA RM L53G13a, 1953.

10. Kuhn, Richard E., Wiggins, James W., and Byrnes, Andrew L., Jr.: Wind-Tunnel Investigation of the Effect of a Fence and a Leading-Edge Notch on the Aerodynamic Loading Characteristics in Pitch of a 45° Sweptback Wing at High Subsonic Speeds. NACA RM L53H24, 1953.

[redacted]

11. Hieser, Gerald.: An Investigation at Transonic Speeds of the Effects of Fences, Drooped Nose, and Vortex Generators on the Aerodynamic Characteristics of a Wing-Fuselage Combination Having a 6-Percent-Thick, 45° Sweptback Wing. NACA RM L53B04, 1953.

12. Wiggins, James W., and Kuhn, Richard E.: Wind-Tunnel Investigation of the Effects of Steady Rolling on the Aerodynamic Loading Characteristics of a 45° Sweptback Wing at High Subsonic Speeds. NACA RM L53J01a, 1953.

13. Fisher, Lewis R.: Approximate Corrections for the Effects of Compressibility on the Subsonic Stability Derivatives of Swept Wings. NACA TN 1854, 1949.

14. Goodman, Alex, and Adair, Glenn H.: Estimation of the Damping in Roll of Wings Through the Normal Flight Range of Lift Coefficient. NACA TN 1924, 1949.

15. Wiggins, James W.: Wind-Tunnel Investigation at High Subsonic Speeds To Determine the Rolling Derivatives of Two Wing-Fuselage Combinations Having Triangular Wings, Including a Semiempirical Method of Estimating the Rolling Derivatives. NACA RM L53L18a, 1954.

16. Goodman, Alex, and Fisher, Lewis R.: Investigation at Low Speeds of the Effect of Aspect Ratio and Sweep on Rolling Stability Derivatives of Untapered Wings. NACA Rep. 968, 1950. (Supersedes NACA TN 1835.)

17. Ribner, Herbert S.: The Stability Derivatives of Low-Aspect-Ratio Triangular Wings at Subsonic and Supersonic Speeds. NACA TN 1423, 1947.

18. Toll, Thomas A., and Queijo, M. J.: Approximate Relations and Charts for Low-Speed Stability Derivatives of Swept Wings. NACA TN 1581, 1948.

19. Letko, William, and Wolhart, Walter D.: Effect of Sweepback on the Low-Speed Static and Rolling Stability Derivatives of Thin Tapered Wings of Aspect Ratio 4. NACA RM L9F14, 1949.

20. Letko, William, and Brewer, Jack D.: Effect of Airfoil Profile of Symmetrical Sections on the Low-Speed Rolling Derivatives of 45° Sweptback-Wing Models of Aspect Ratio 2.61. NACA RM L8L31a, 1949.

[redacted]

TABLE I.- FUSELAGE ORDINATES

[Basic fineness ratio 12, actual fineness ratio 9.8 achieved by cutting off rear portion of body]

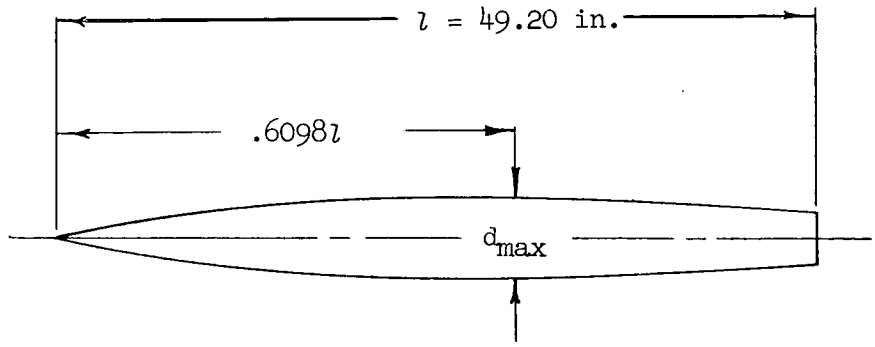

Ordinates, percent length	
Station	Radius
0	0
.61	.28
.91	.36
1.52	.52
3.05	.88
6.10	1.47
9.15	1.97
12.20	2.40
18.29	3.16
24.39	3.77
30.49	4.23
36.59	4.56
42.68	4.80
48.78	4.95
54.88	5.05
60.98	5.08
67.07	5.04
73.17	4.91
79.27	4.69
85.37	4.34
91.46	3.81
100.00	3.35
Leading-edge radius = 0.0006l	

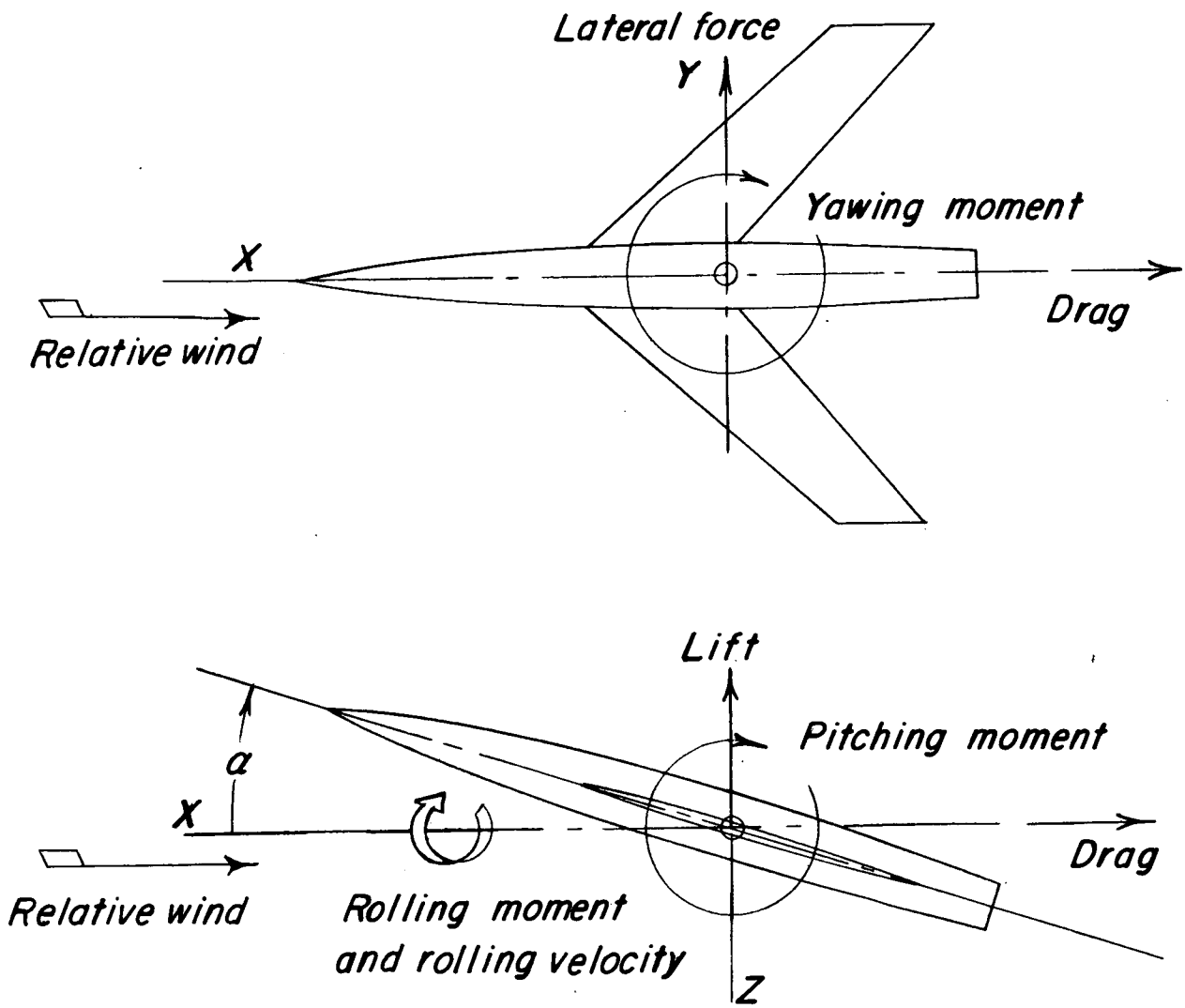

Figure 1.- System of axes used showing positive direction of forces, moments, angles, and velocities.

Fuselage:

Length	49.2 in.
Max. diam.	5 in.
Position of max. diam.	30 in.

Wing:

Area	2.25 sq ft
Span	3.0 ft.
Chord	
Tip	6.75 in.
Root	11.25 in.
Mean aerodynamic chord	.765 ft
Aspect ratio	4.0
Taper ratio	0.6
Incidence	0
Dihedral	0
Airfoil section parallel to fuselage ℄	NACA 65A006

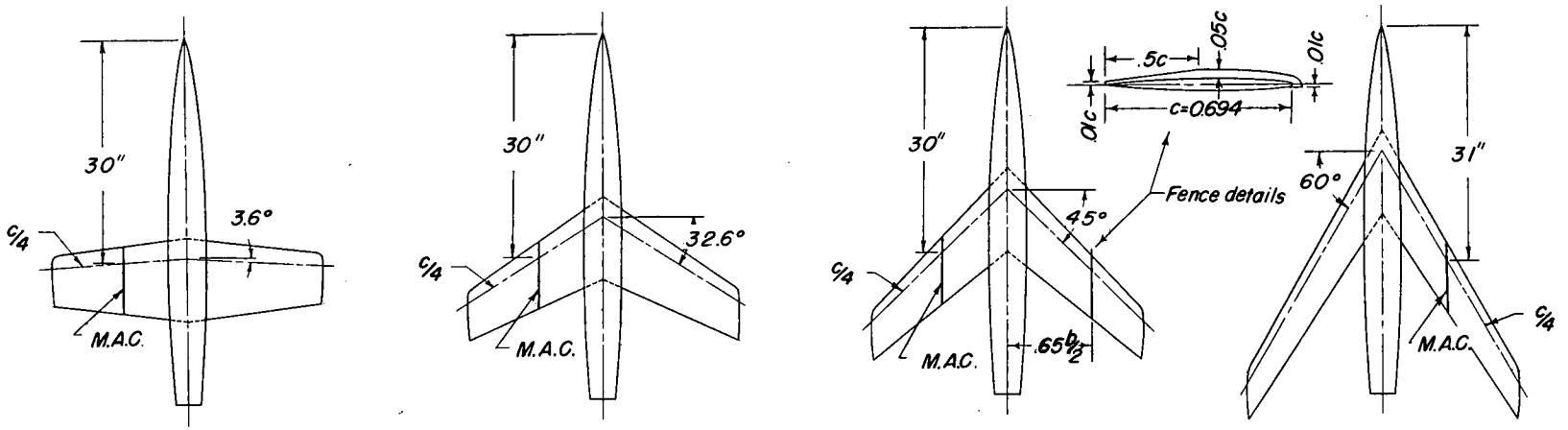

Figure 2.- Sketch of four wing-fuselage configurations.

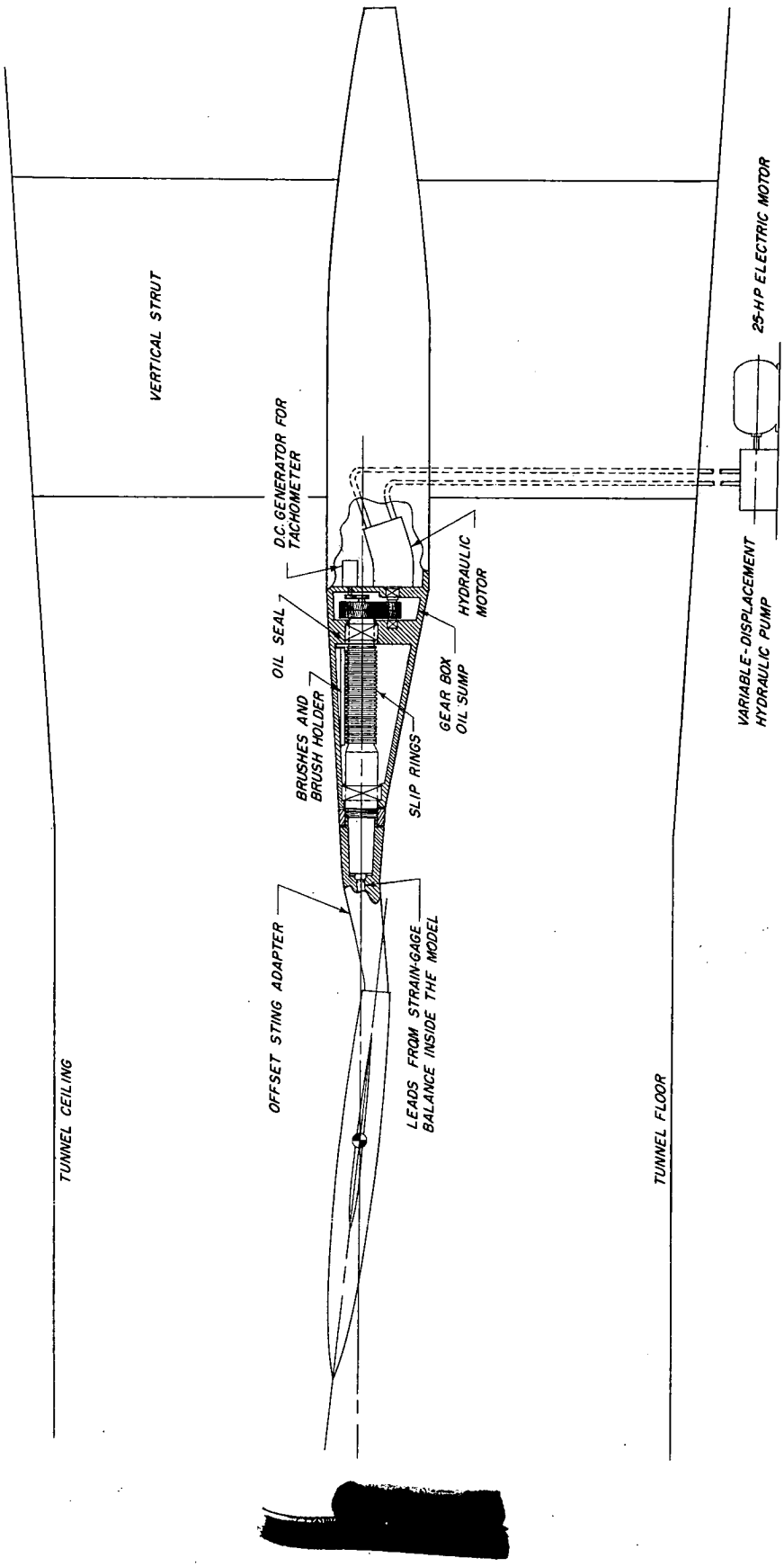

Figure 3.- General arrangement of forced-roll sting-support system.

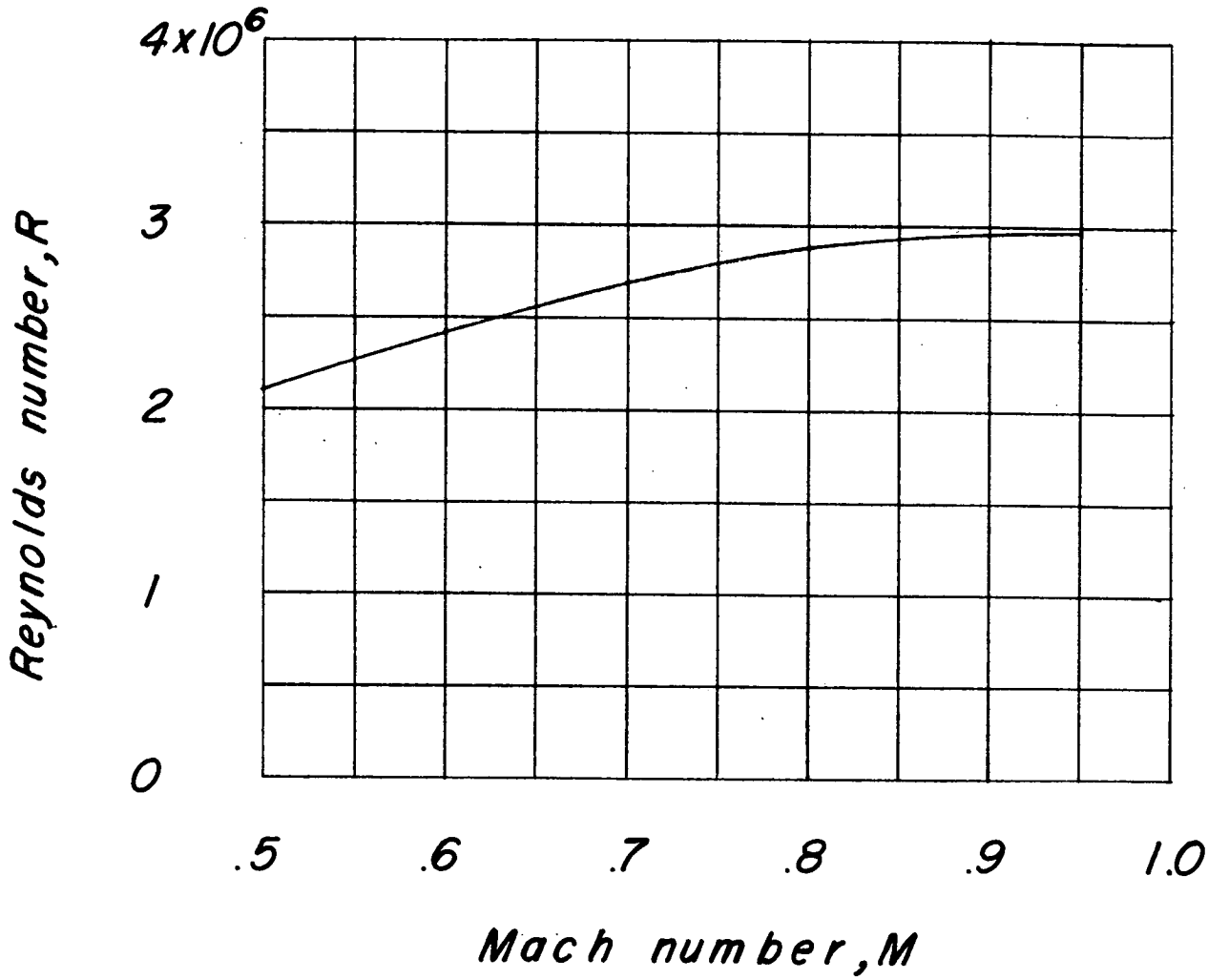

Figure 4.- Variation of mean test Reynolds number with Mach number for wings tested.

[redacted]

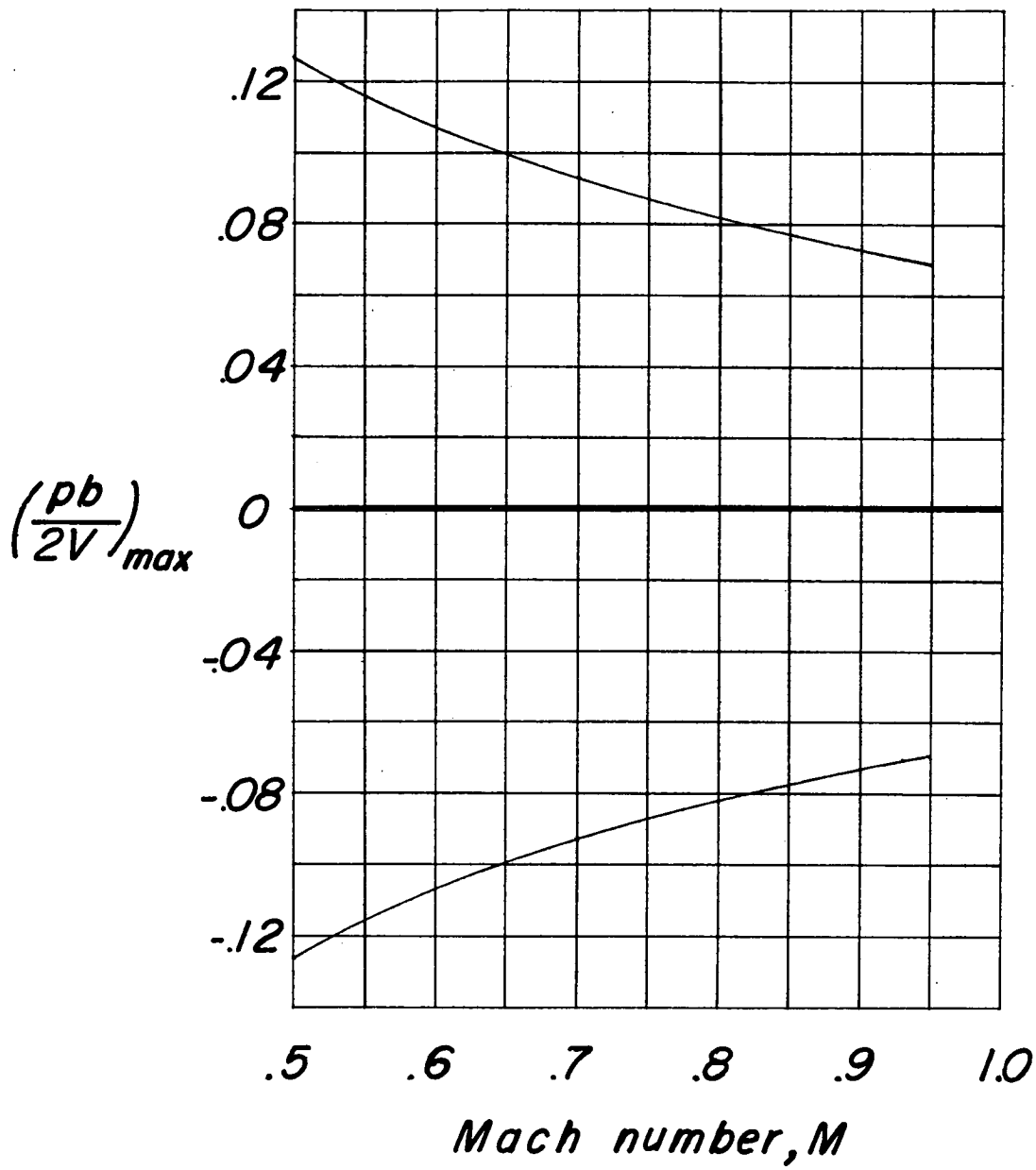

Figure 5.- Variation of maximum test values of pb/2V with Mach number for wings tested.

[redacted]

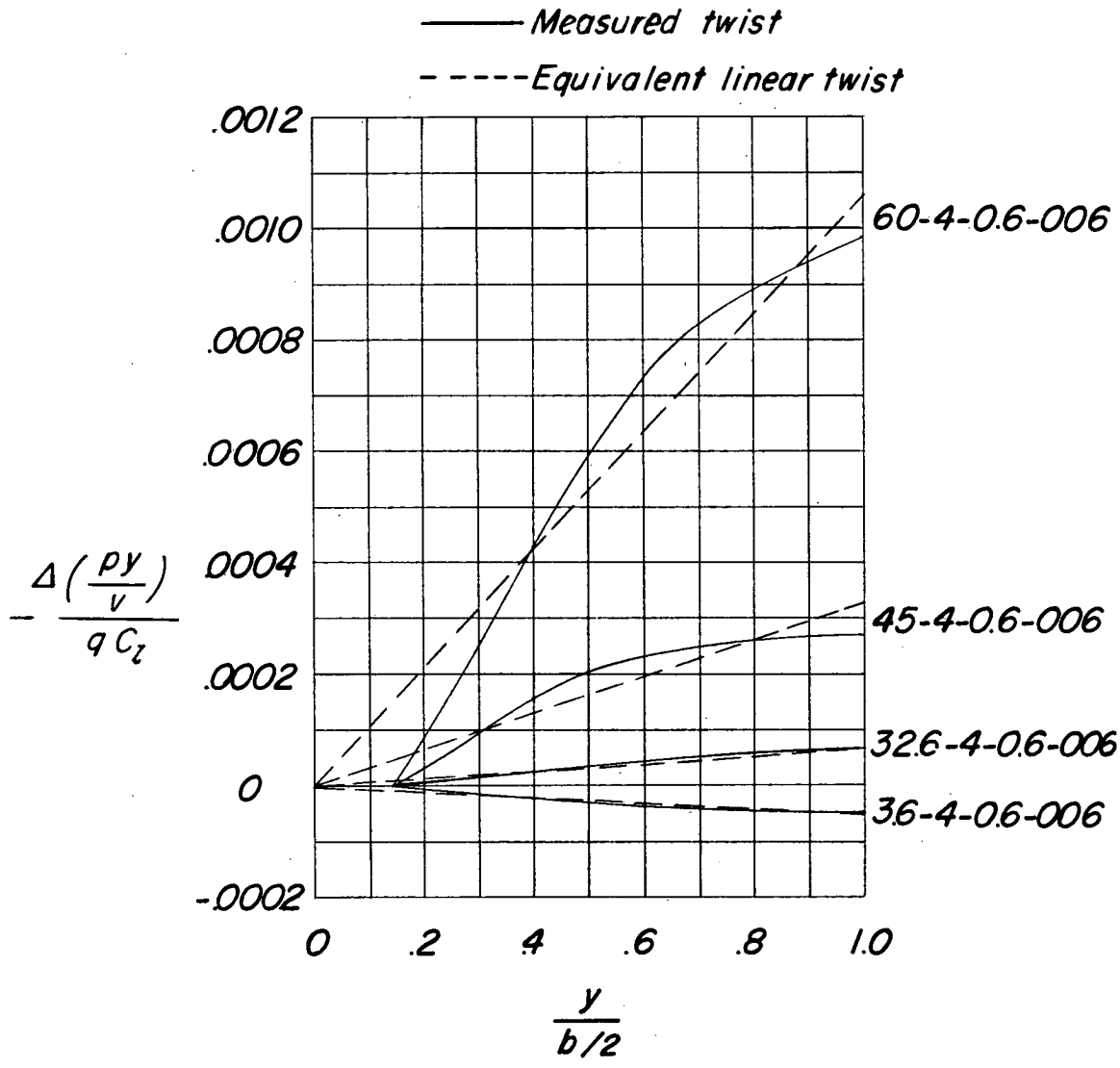

Figure 6.- Aeroelastic characteristics for wings.

[redacted]

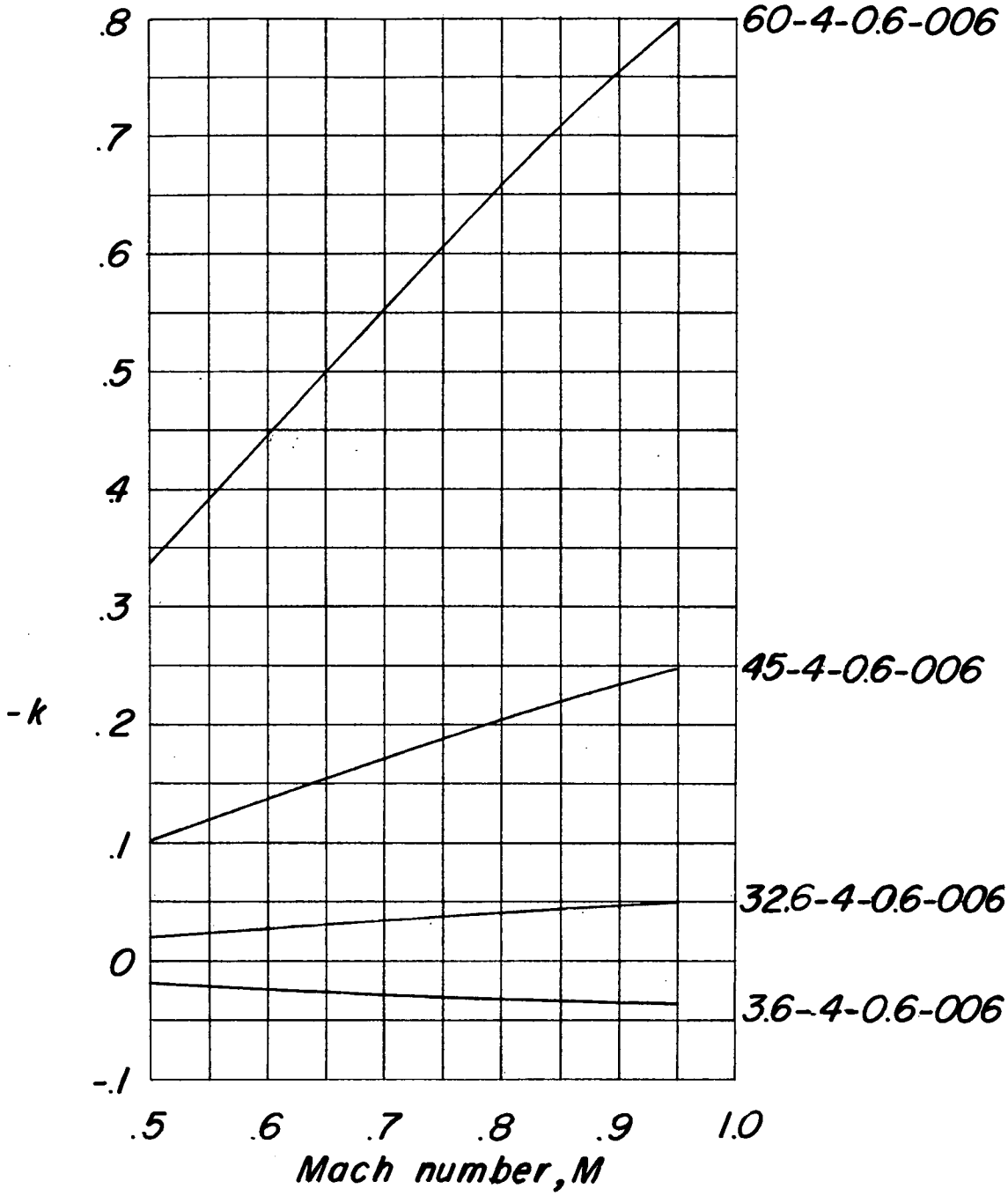

Figure 7.- Aeroelastic correction factors for wings tested. $\alpha = 0^{\circ}$.

[redacted]

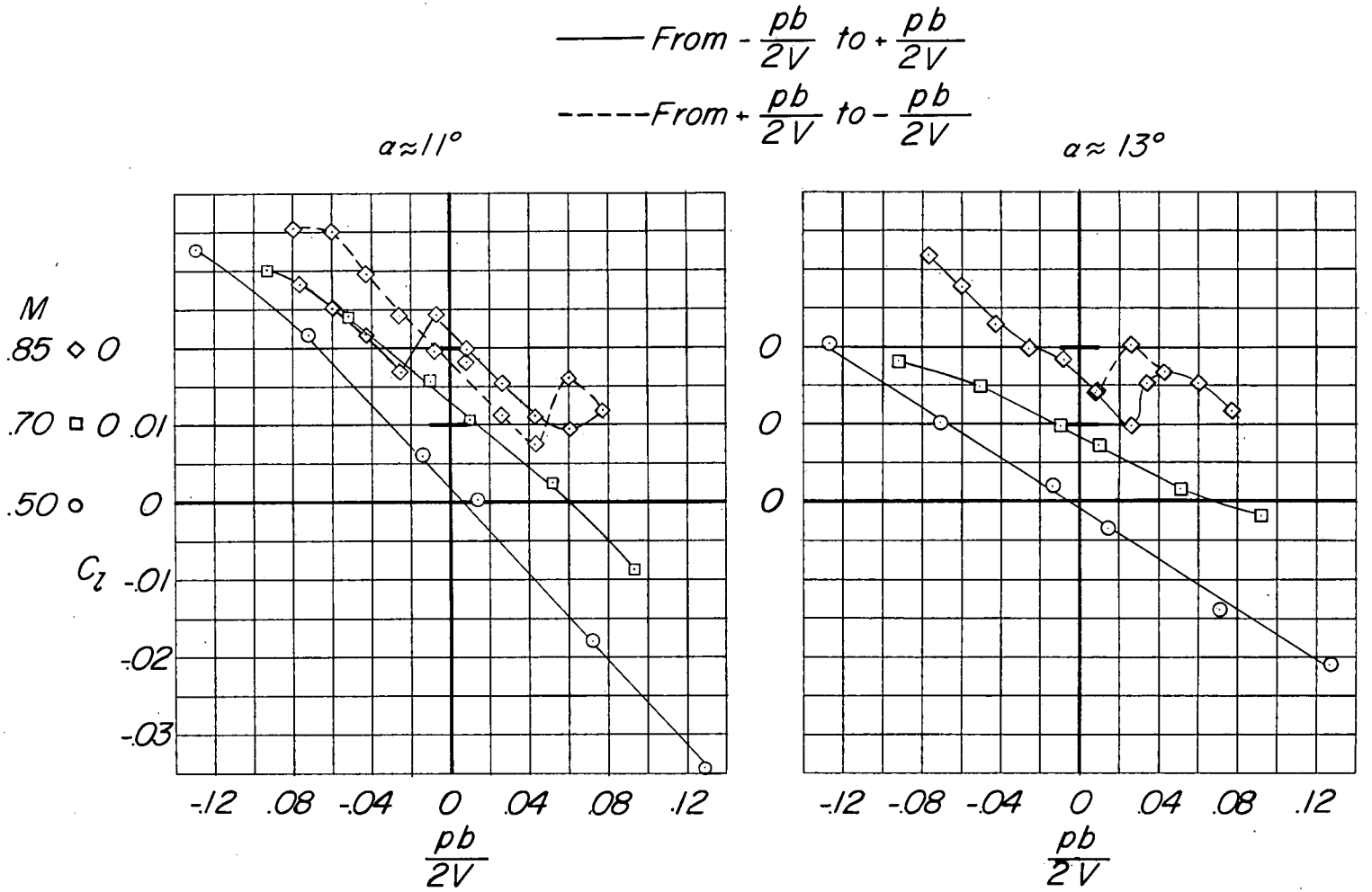

(a) 3.6-4-.6-006 wing.

Figure 8.- Variation of C_l with pb/2V in high test angle-of-attack range for three of wings investigated.

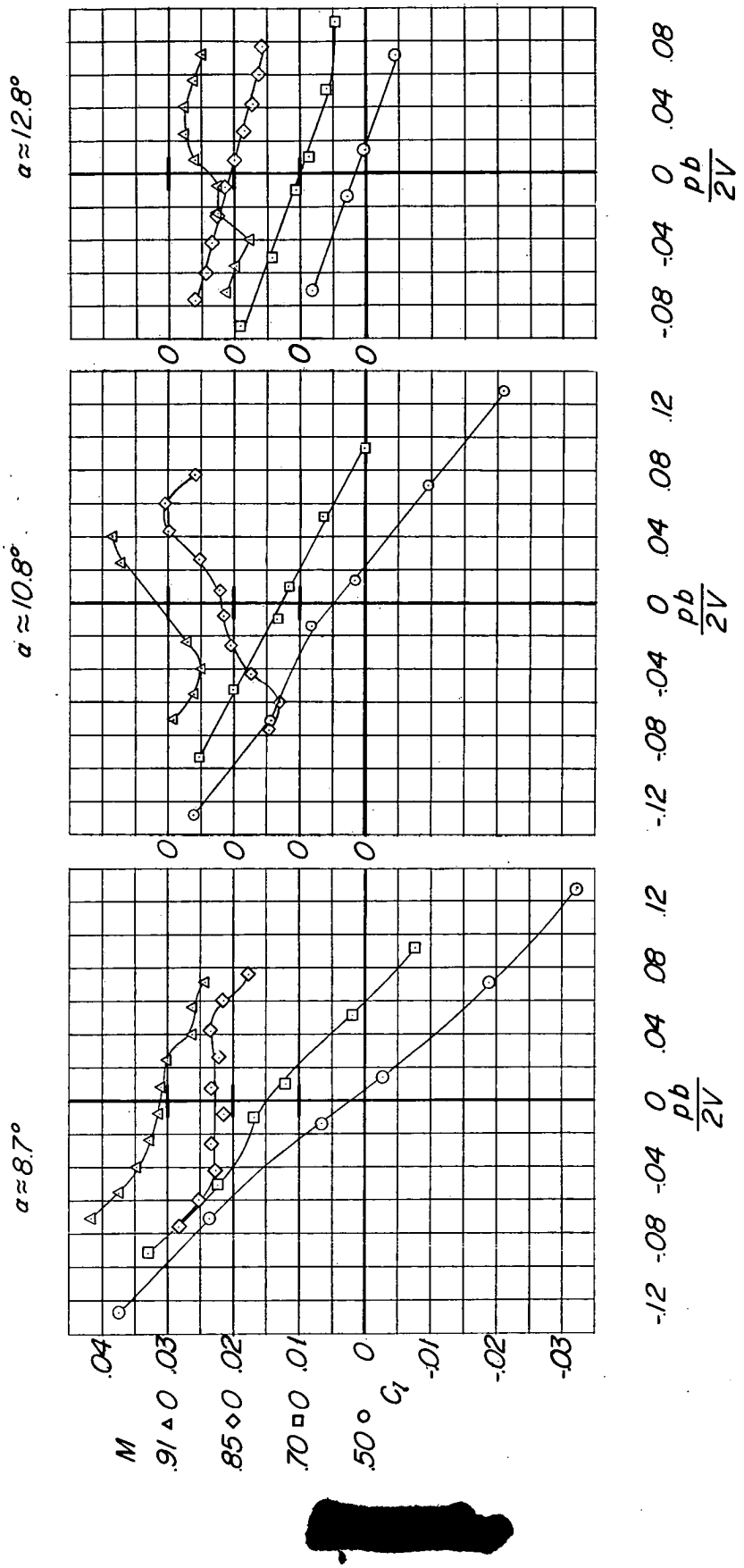

(b) 32.6-4-.6-006 wing.

Figure 8.- Continued.

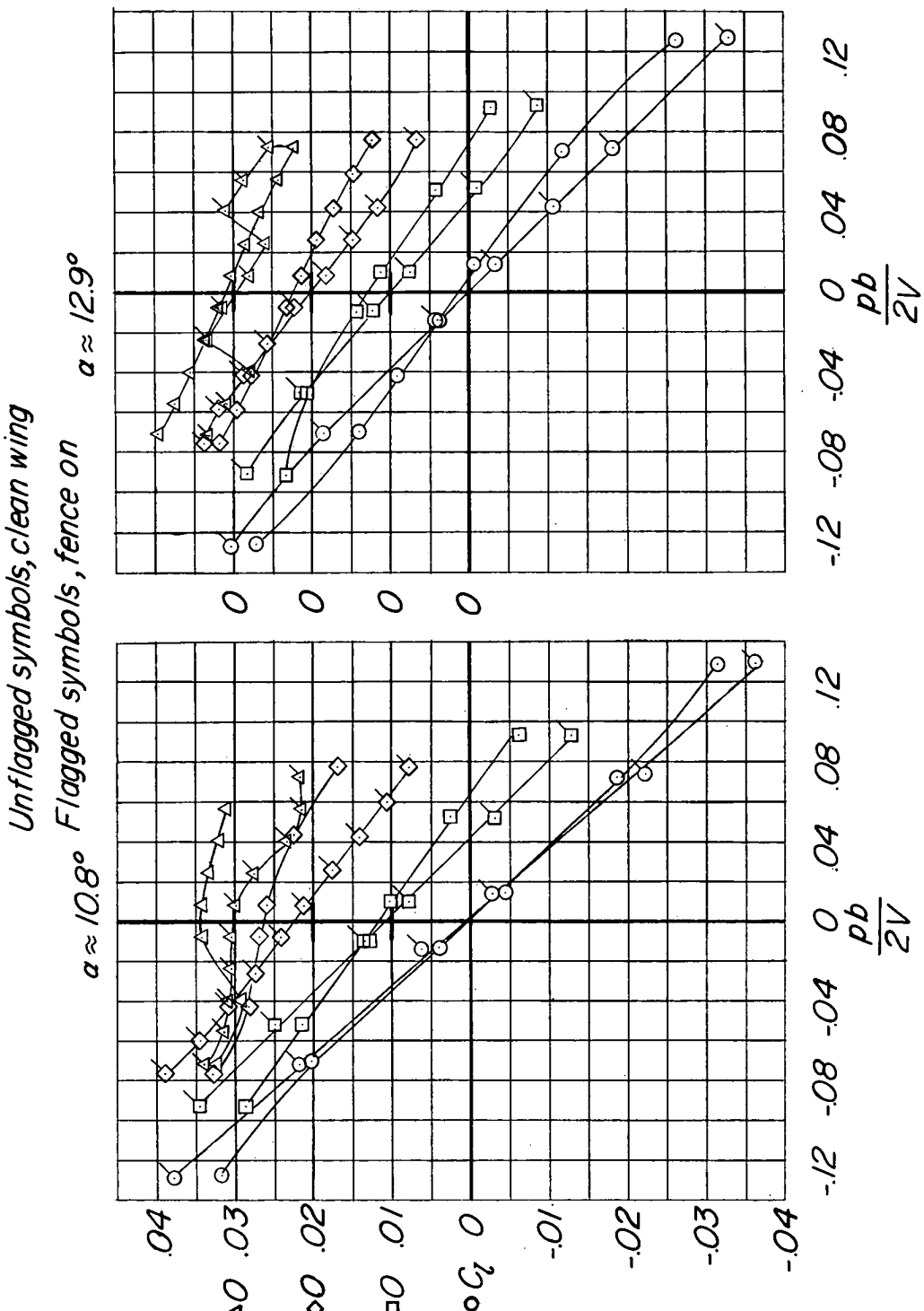

(c) 45-4-.6-006 wing.

Figure 8.- Concluded.

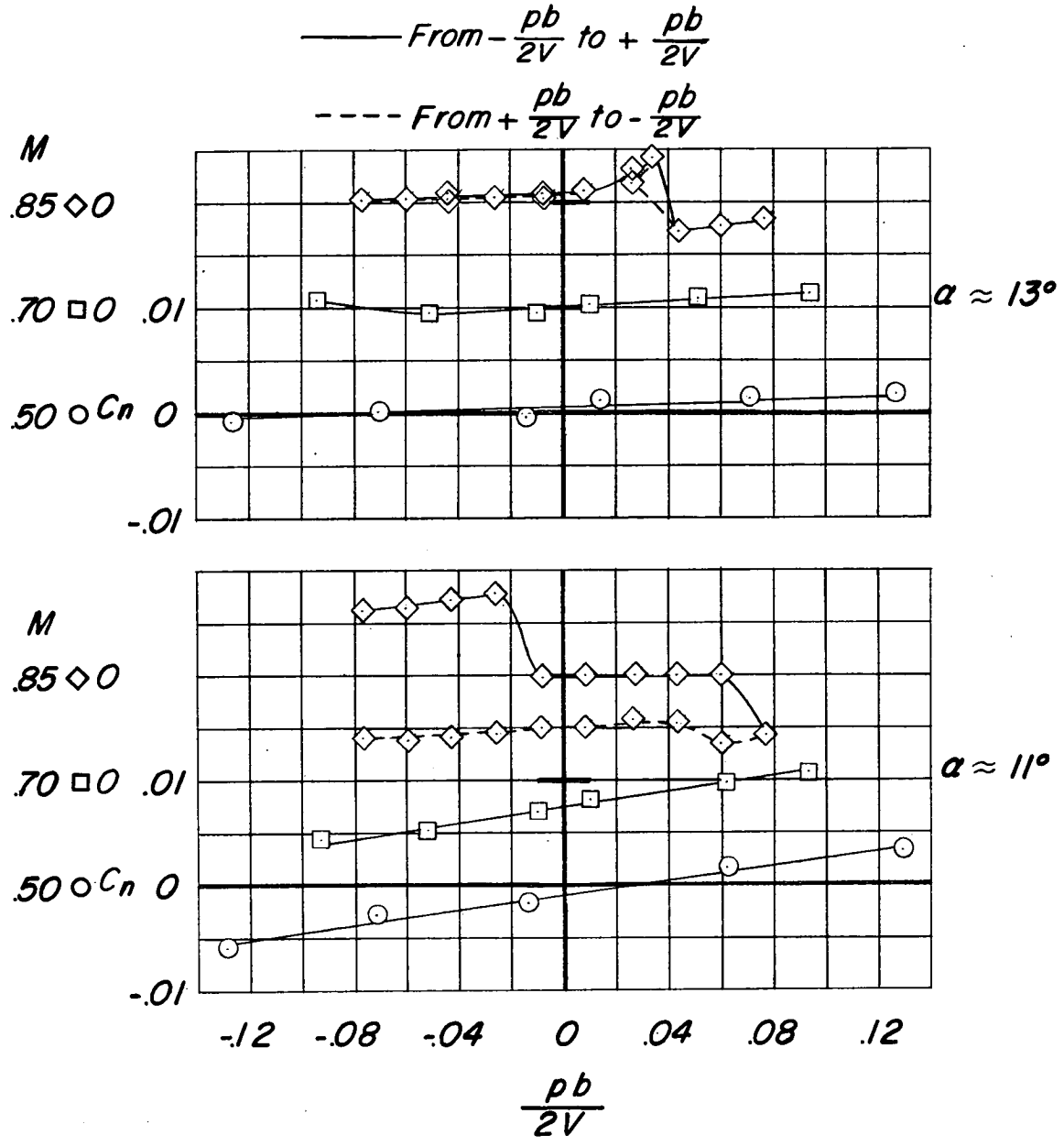

Figure 9.- Variation of yawing moment with wing-tip helix angle pb/2V in high test angle-of-attack range. 3.6-4-.6-006 wing.

[redacted]

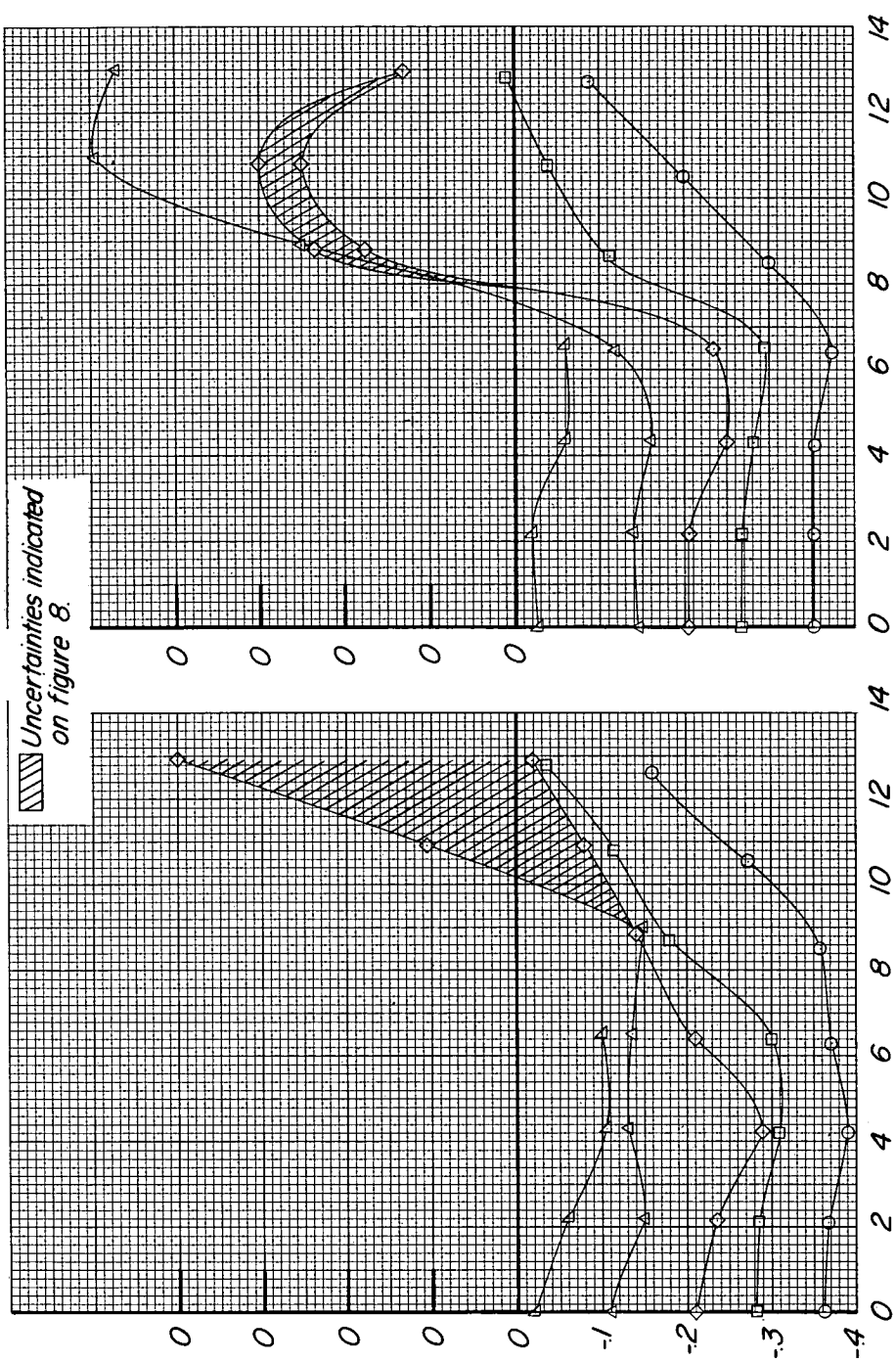

(a) 3.6-4-.6-006 wing. (b) 32.6-4-.6-006 wing.

Figure 10.- Variation of C_{l_p} with angle of attack for wings tested. Data not corrected for aeroelastic distortion.

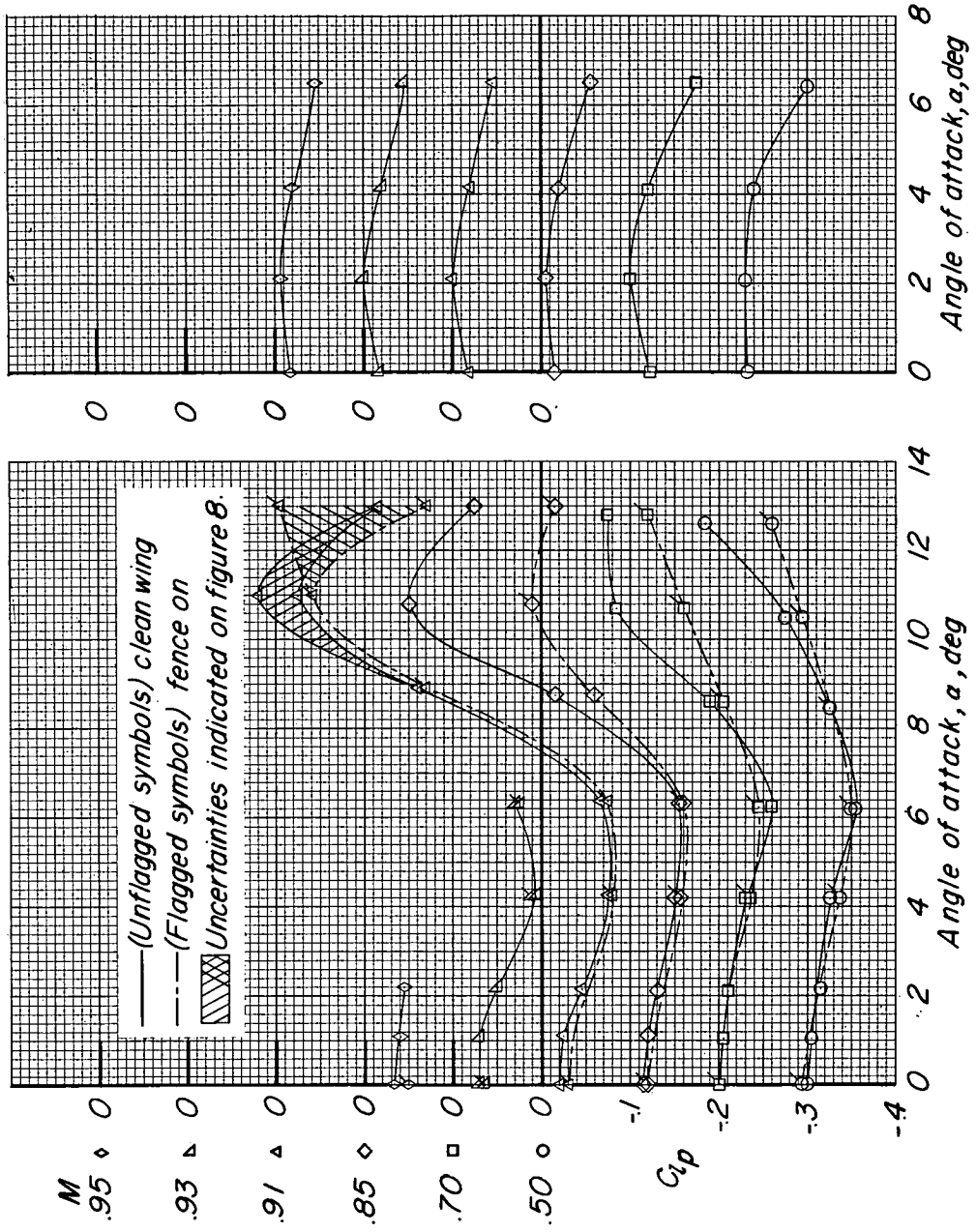

(c) 45-4-.6-006 wing. (d) 60-4-.6-006 wing.

Figure 10.- Concluded.

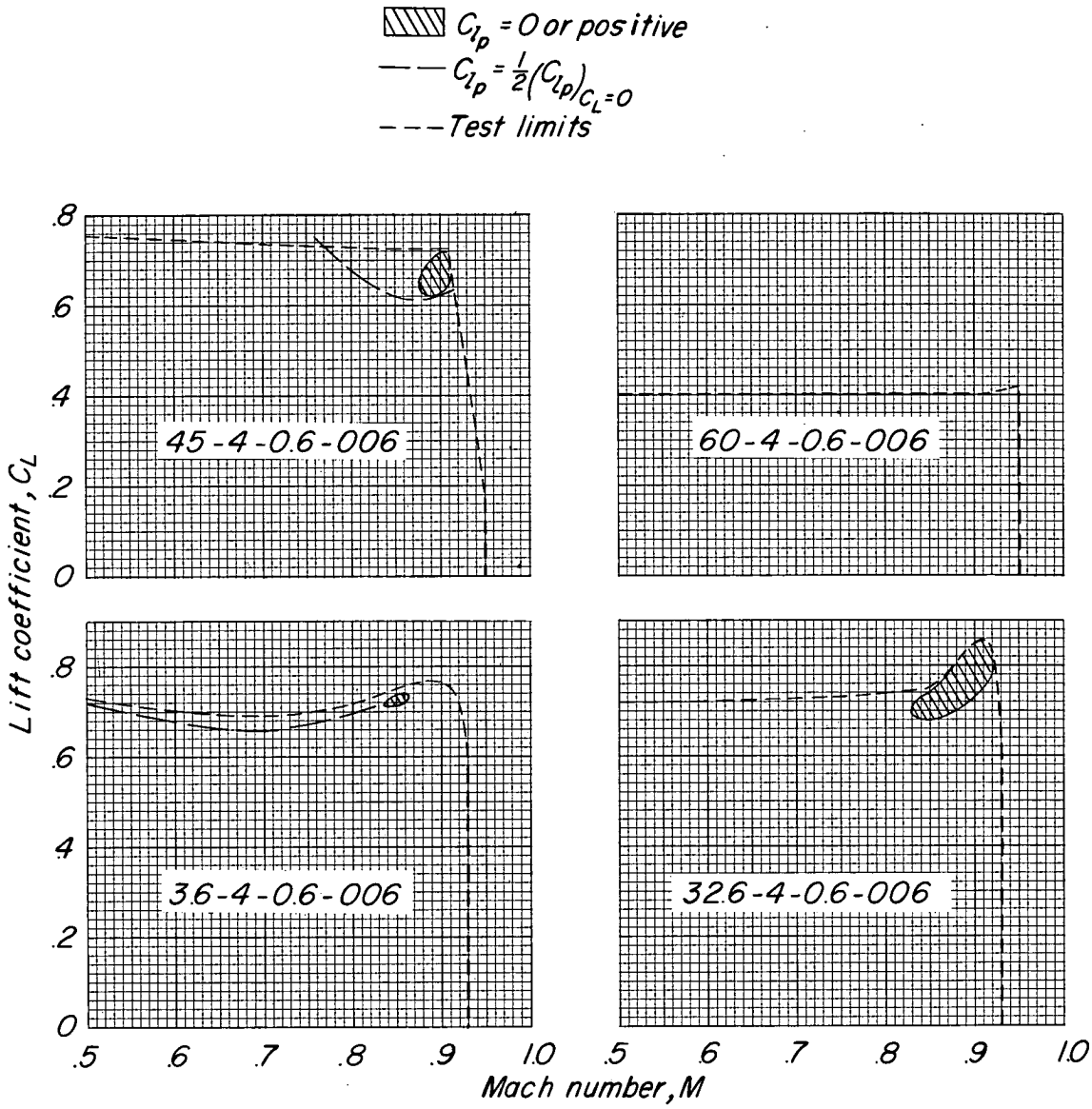

Figure 11.- Boundaries for C_{l_p} for test ranges of lift coefficient and Mach number.

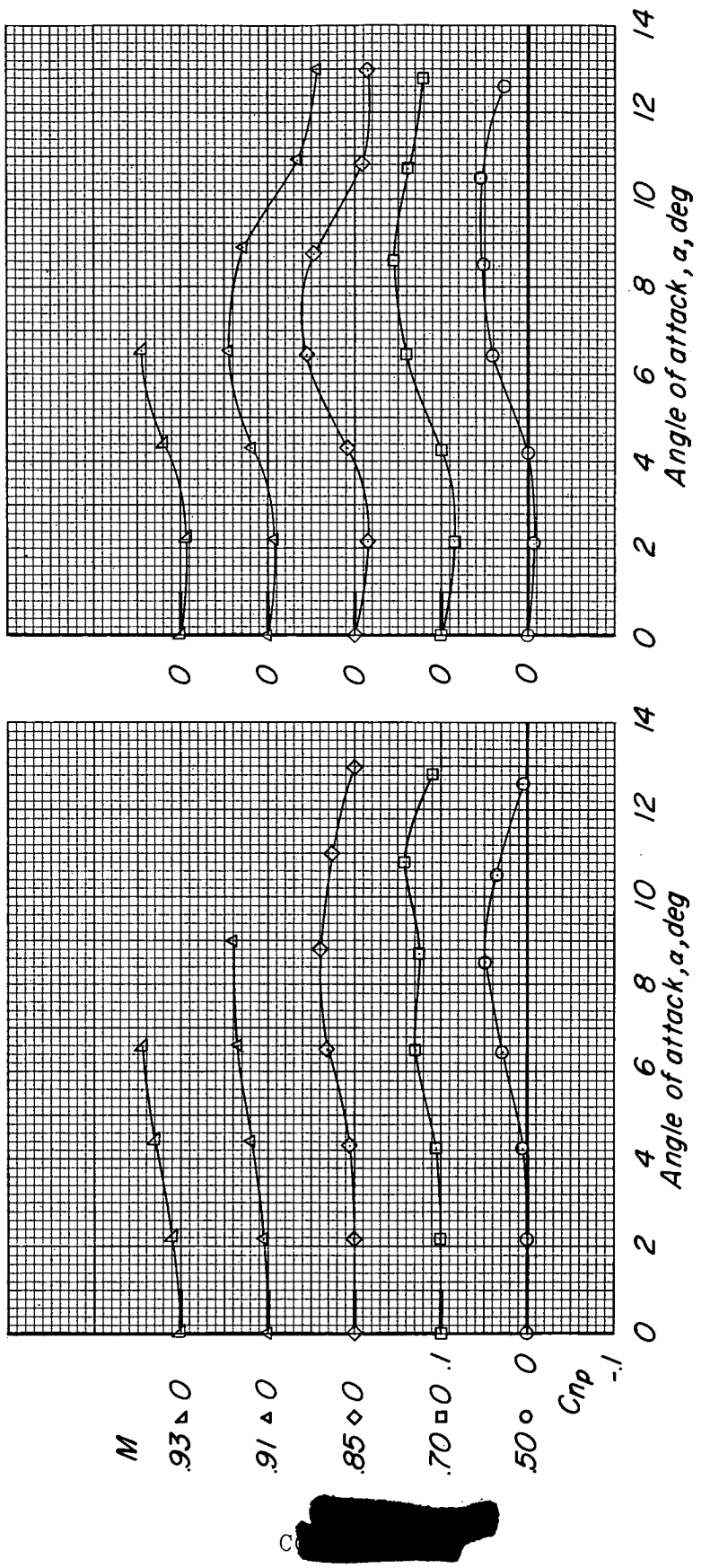

(a) 3.6-4-.6-006 wing. (b) 32.6-4-.6-006 wing.

Figure 12.- Variation of C_{l_p} with angle of attack for wings tested.

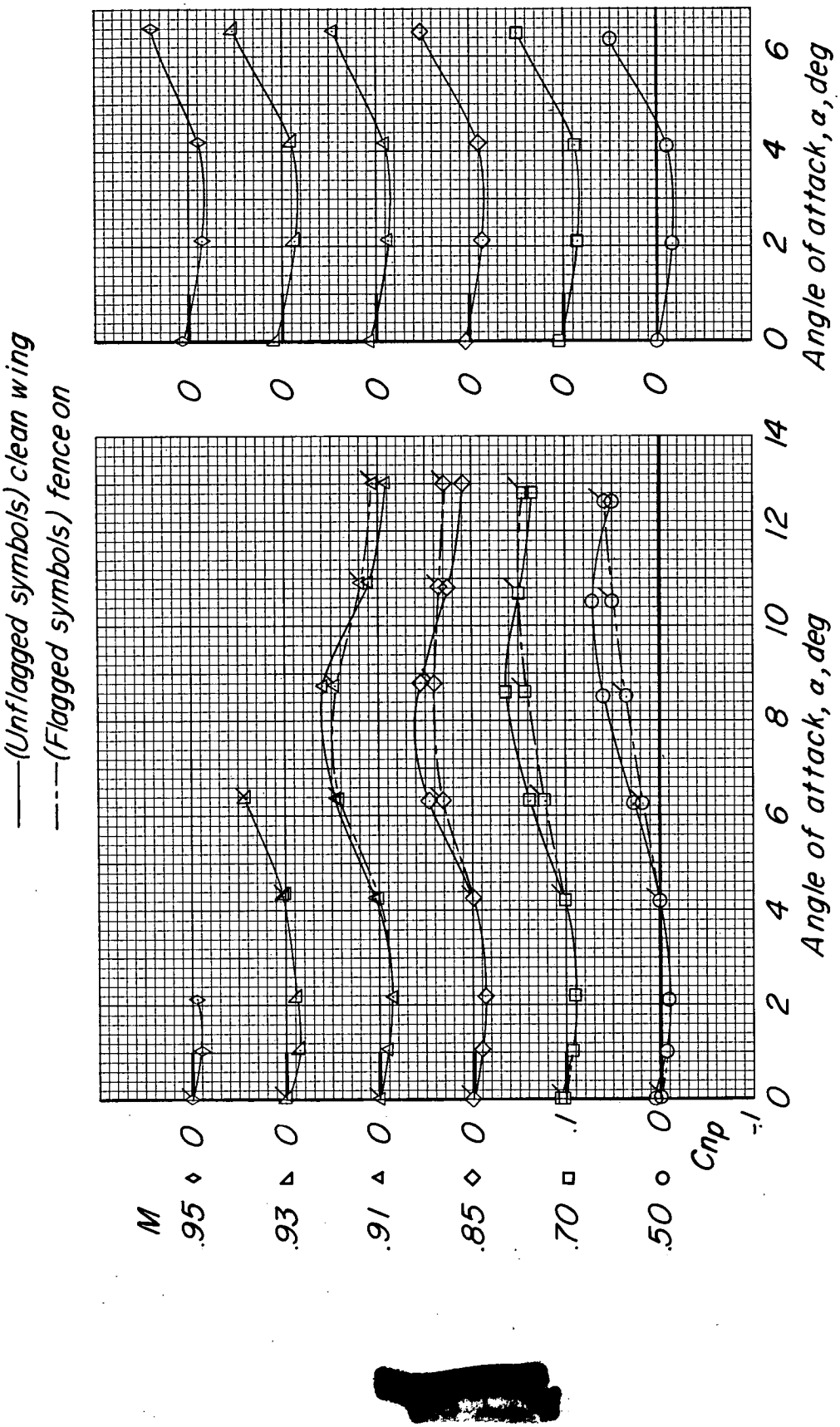

(c) 45-4-.6-006 wing. (d) 60-4-.6-006 wing.

Figure 12.- Concluded.

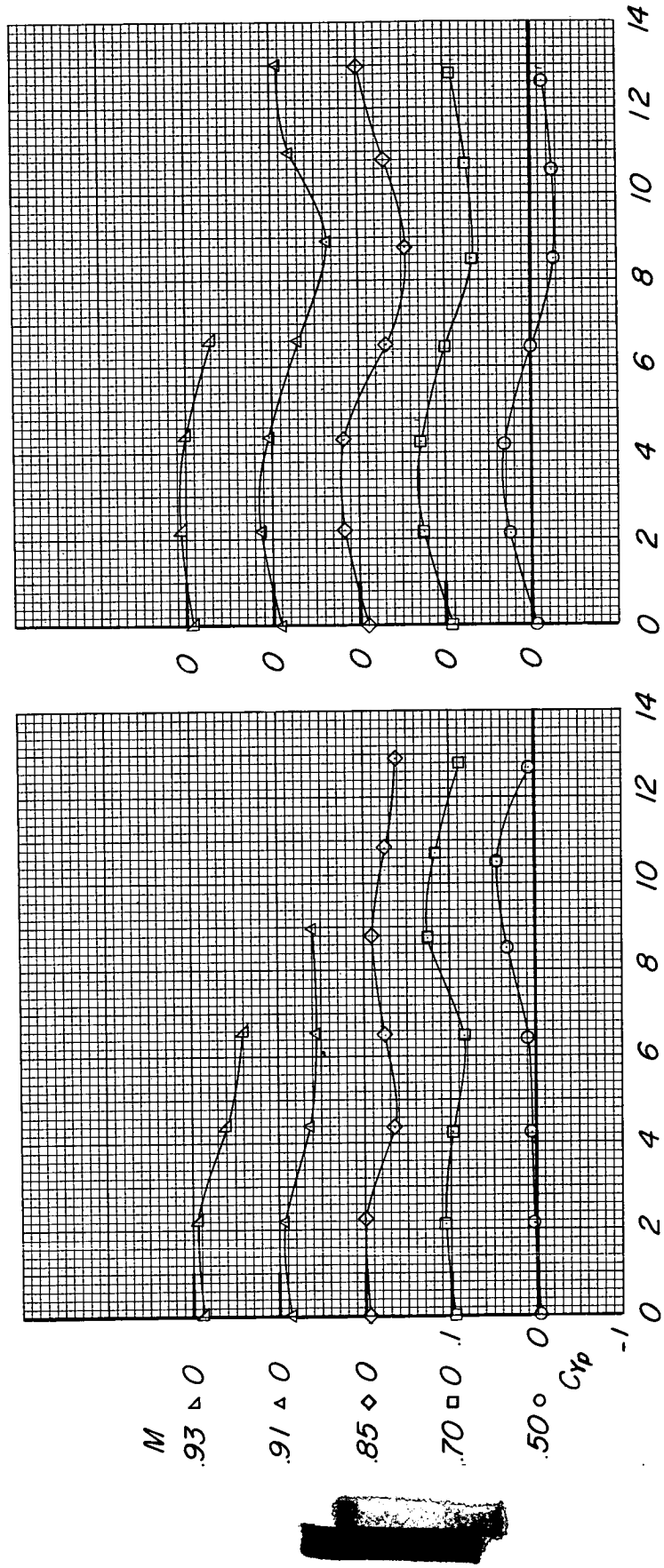

(a) 3.6-4-.6-006 wing. (b) 32.6-4-.6-006 wing.

Figure 13.- Variation of C_{Y_p} with angle of attack for the four wings tested.

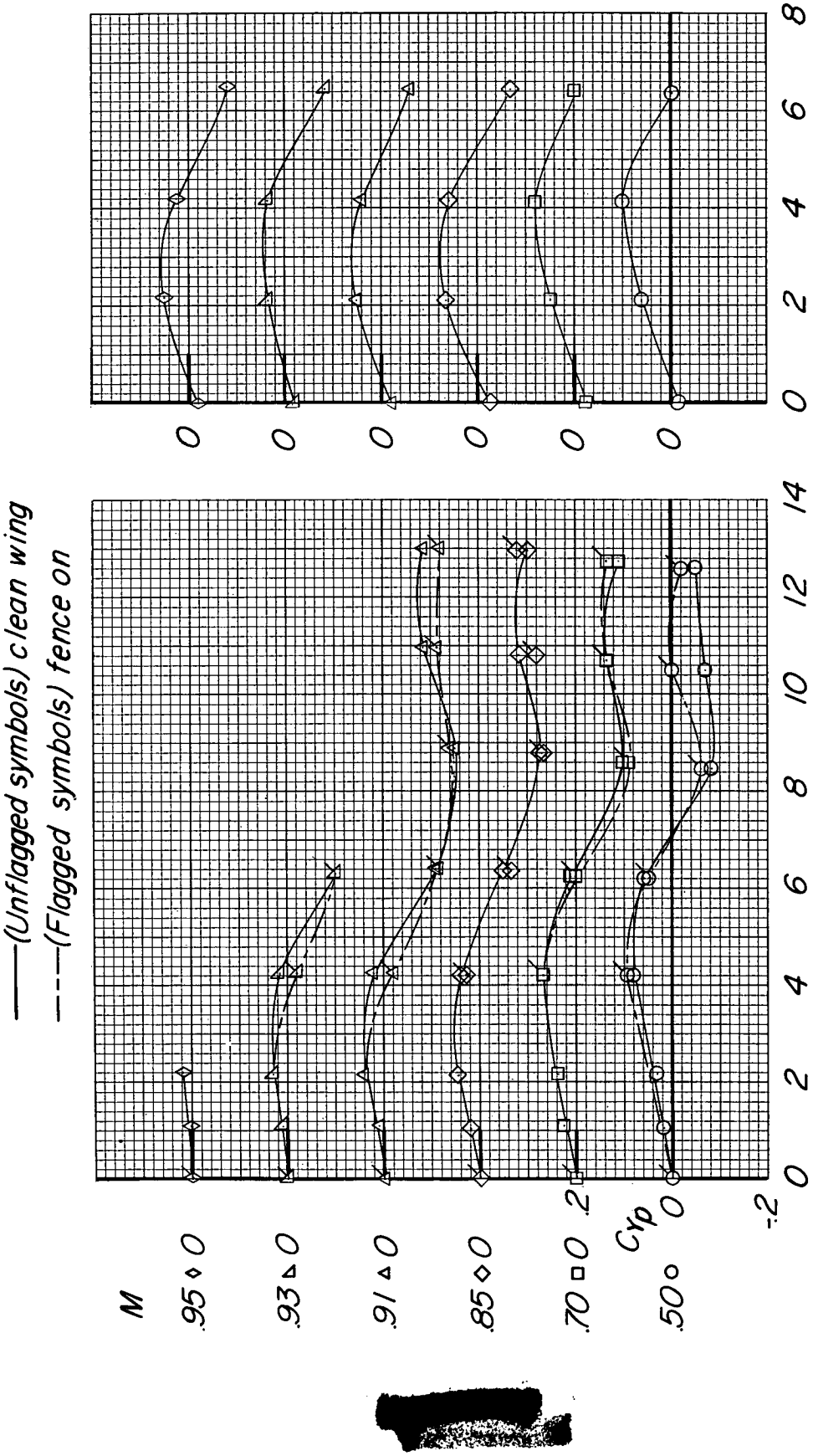

(c) 45-4-.6-006 wing. (d) 60-4-.6-006 wing.

Figure 13.- Concluded.

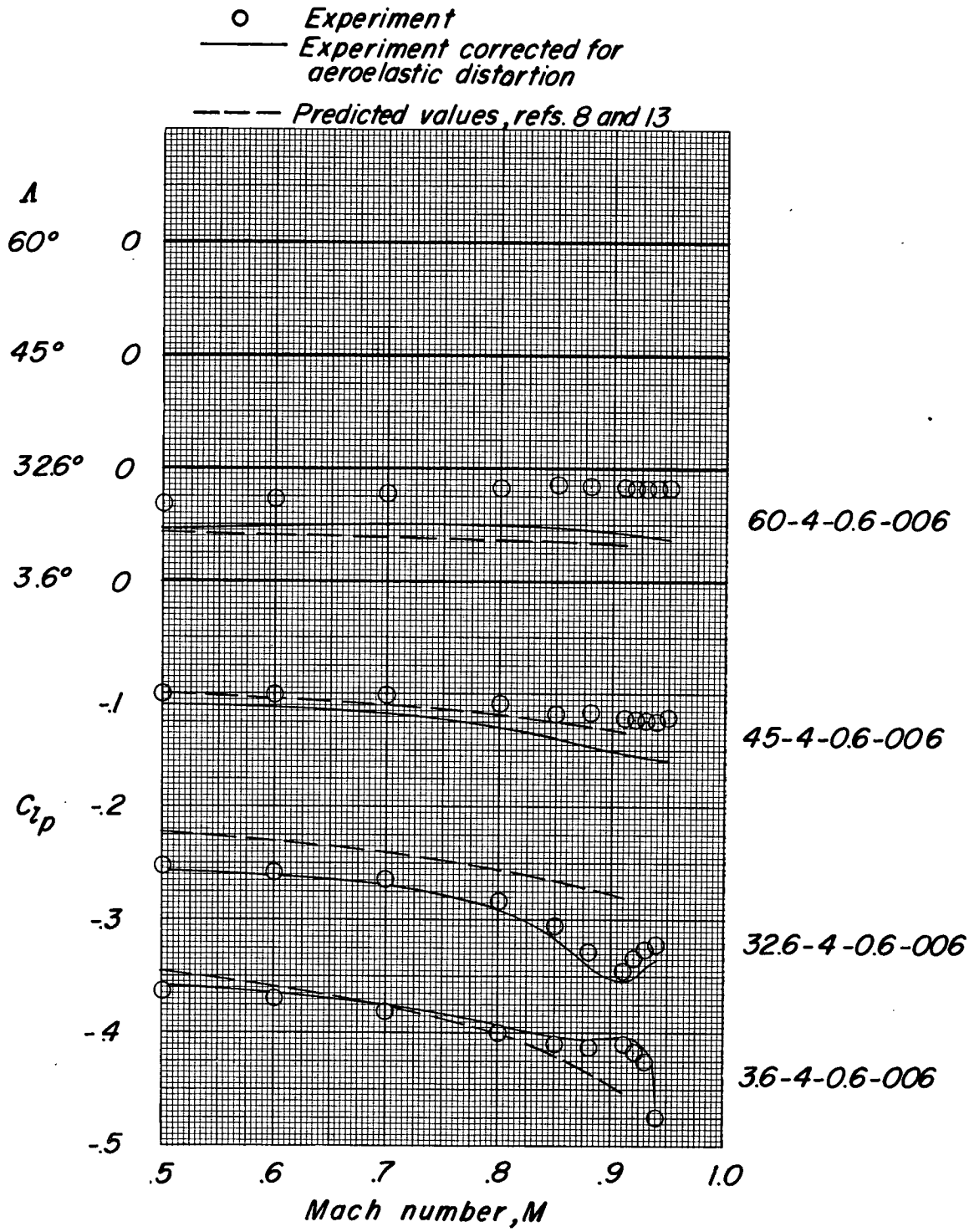

Figure 14.- Comparison of experimental and calculated variation of C_{l_p} with Mach number. $\alpha = 0^{\circ}$.

[redacted]

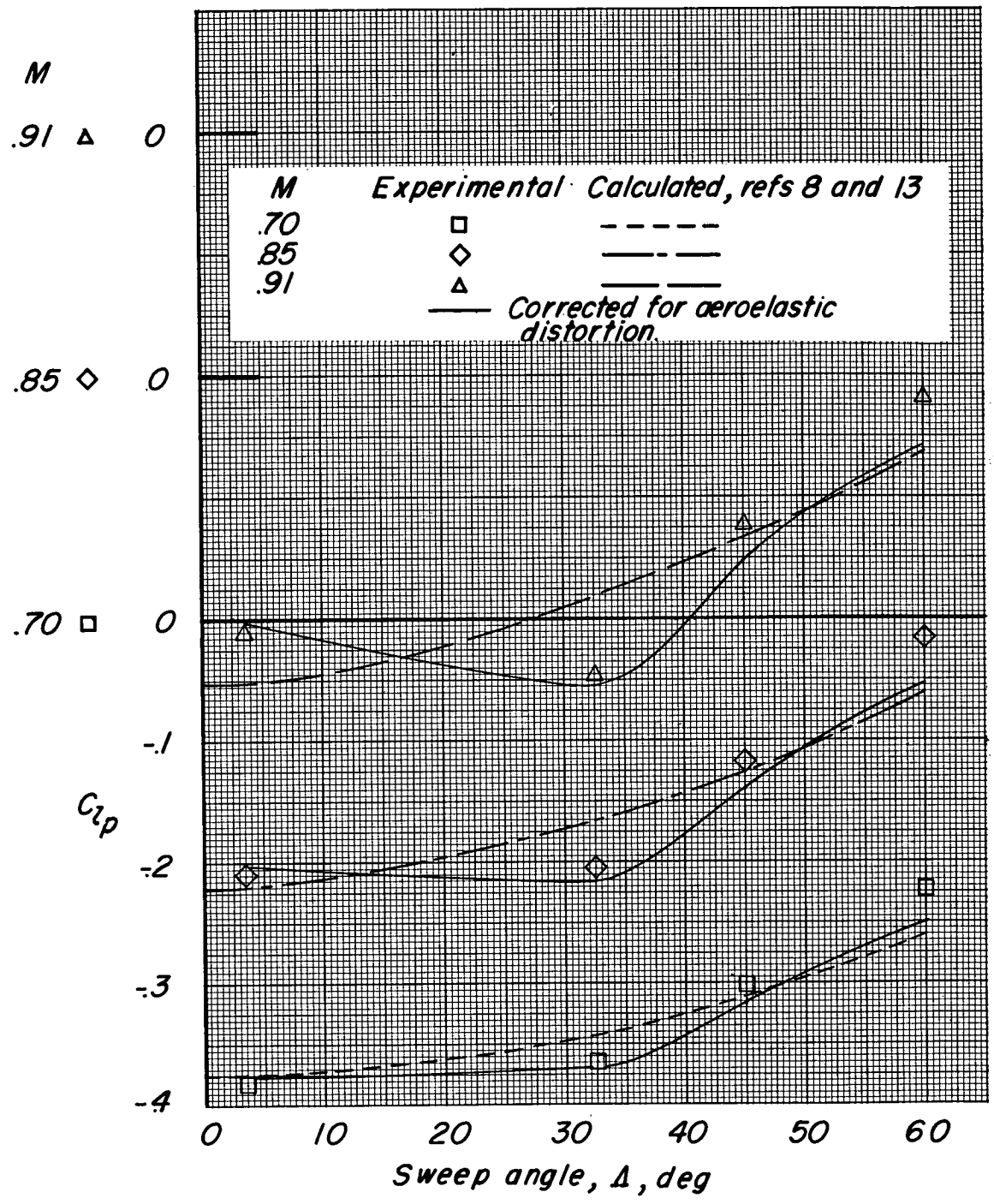

Figure 15.- Comparison of experimental and predicted variation of C_{l_p} with sweep angle. $\alpha = 0^{\circ}$.

[redacted]

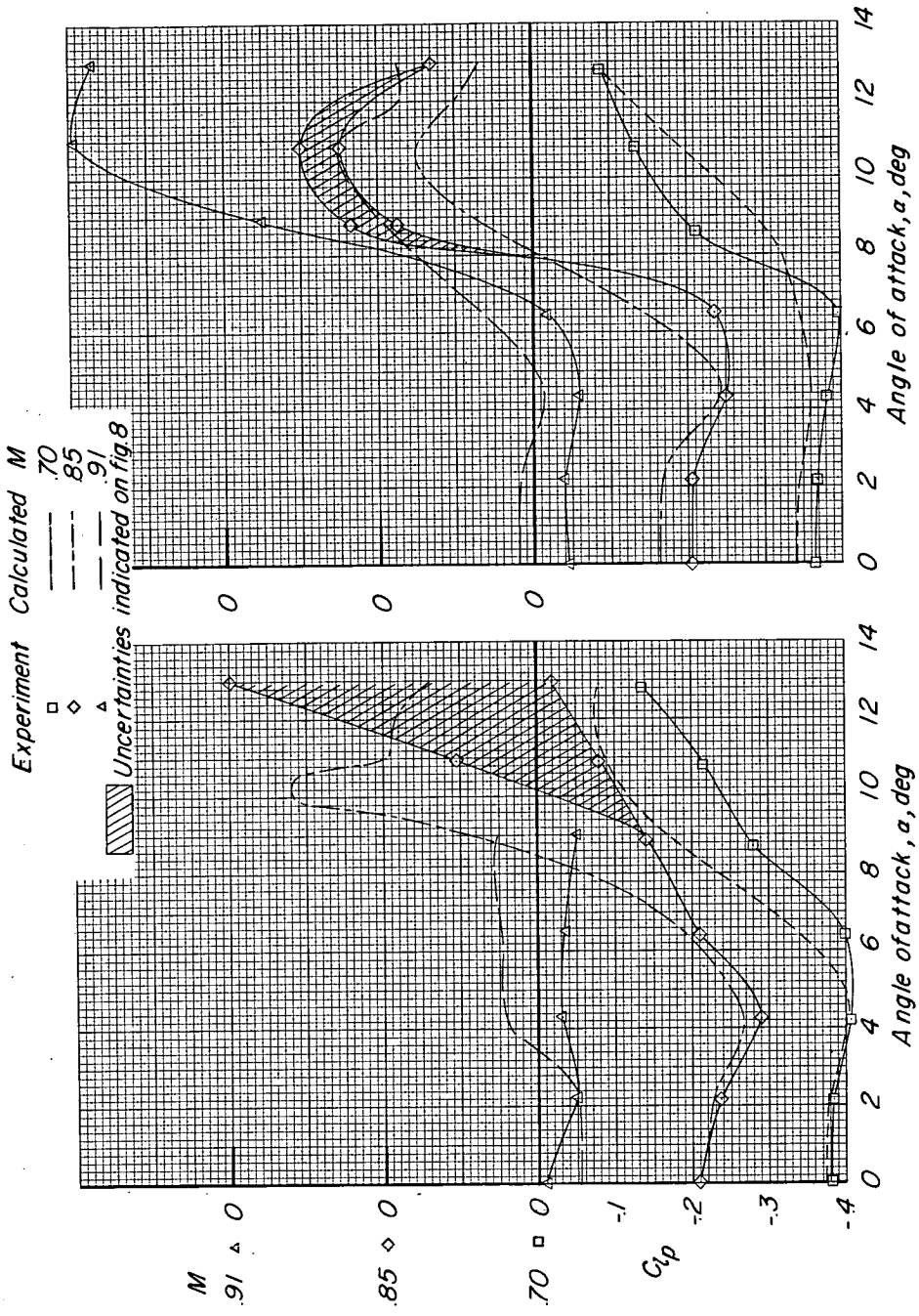

(a) 3.6-4-.6-006 wing. (b) 32.6-4-.6-006 wing.

Figure 16.- Comparison of experimental and calculated variation of C_{l_p} with angle of attack for wings tested. Data not corrected for aeroelastic distortion.

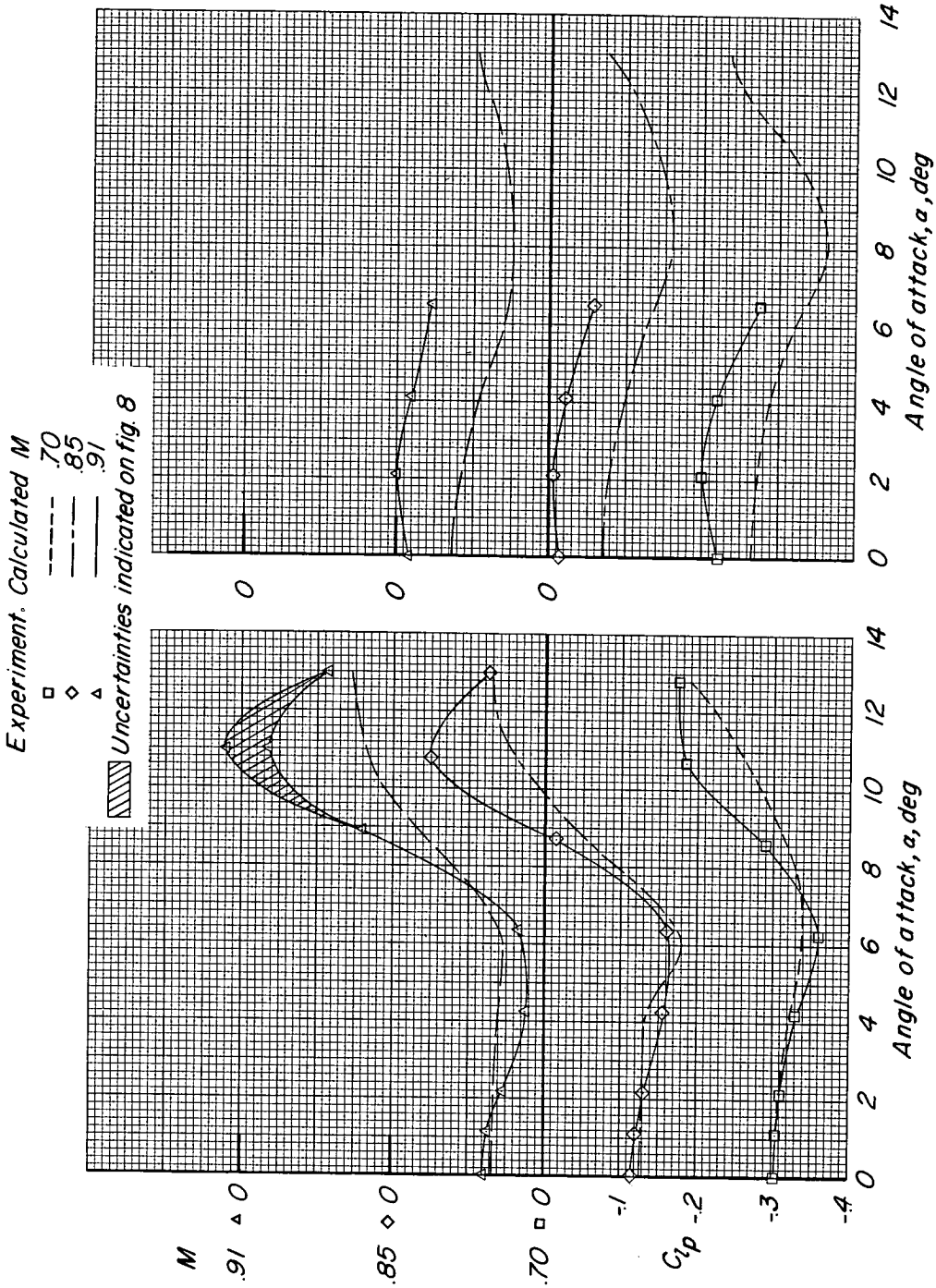

(c) 45-4-.6-006 wing. (d) 60-4-.6-006 wing.

Figure 16.- Concluded.

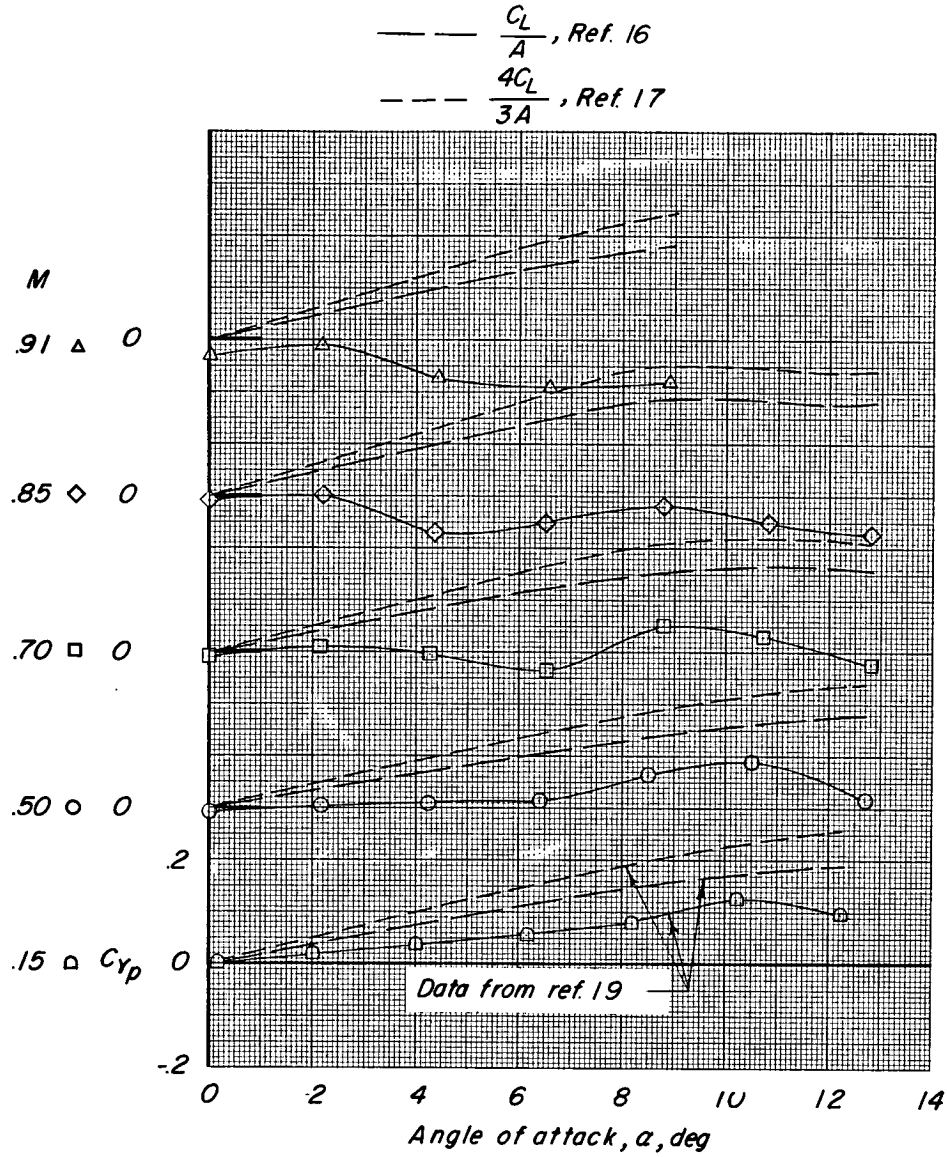

Figure 17.- Comparison of experimental C_{Y_p} with calculated values for 3.6-4-.6-006 wing.

[redacted]

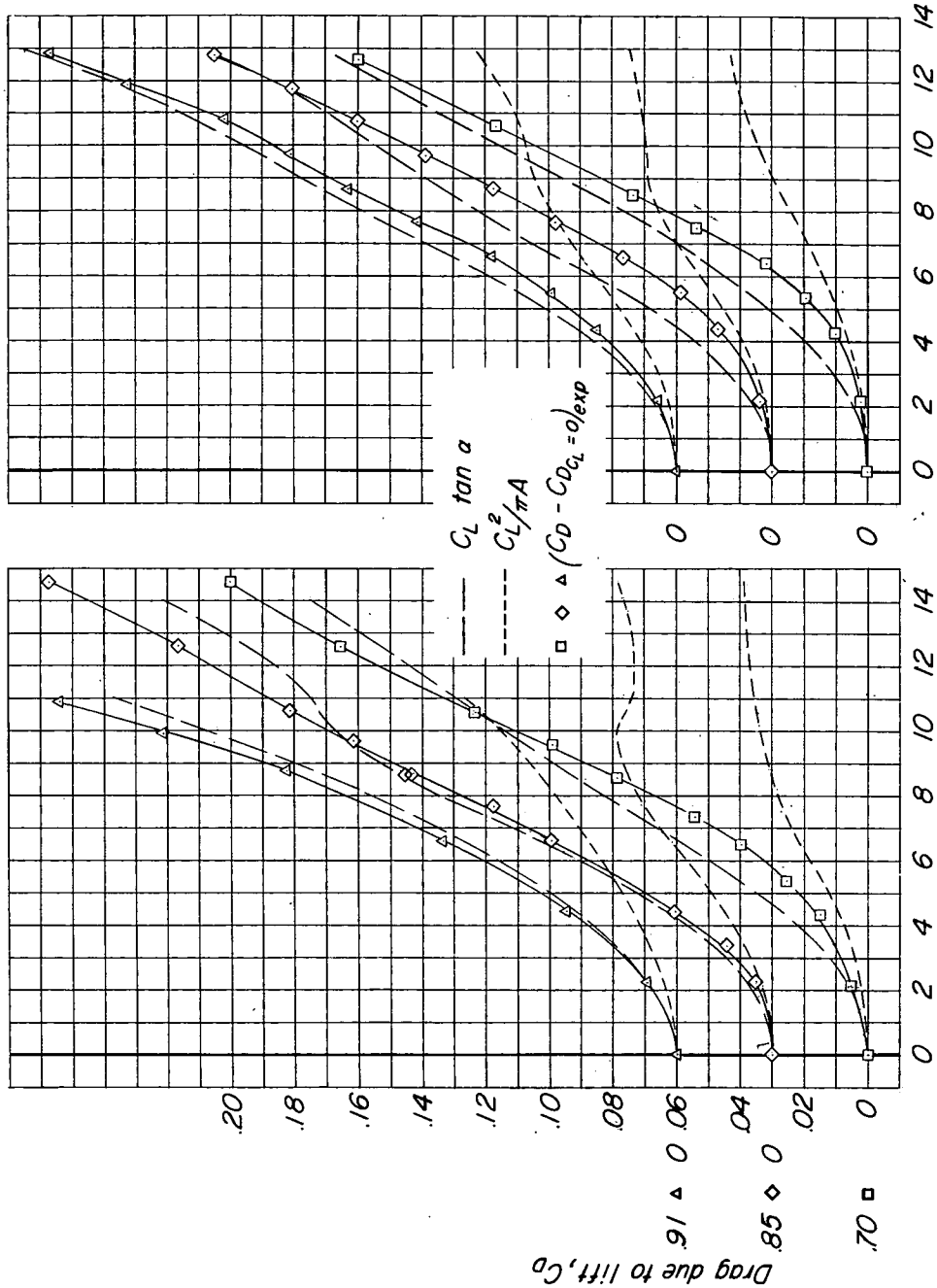
Drag due to lift, C_{D_0}
Angle of attack, α, deg
Angle of attack, α, deg
$C_L \tan \alpha$
$C_L^2/\pi A$
$(C_D - C_{D_{C_L=0}})_{exp}$
.70 □
.85 ◇
.16 △
0
0
0

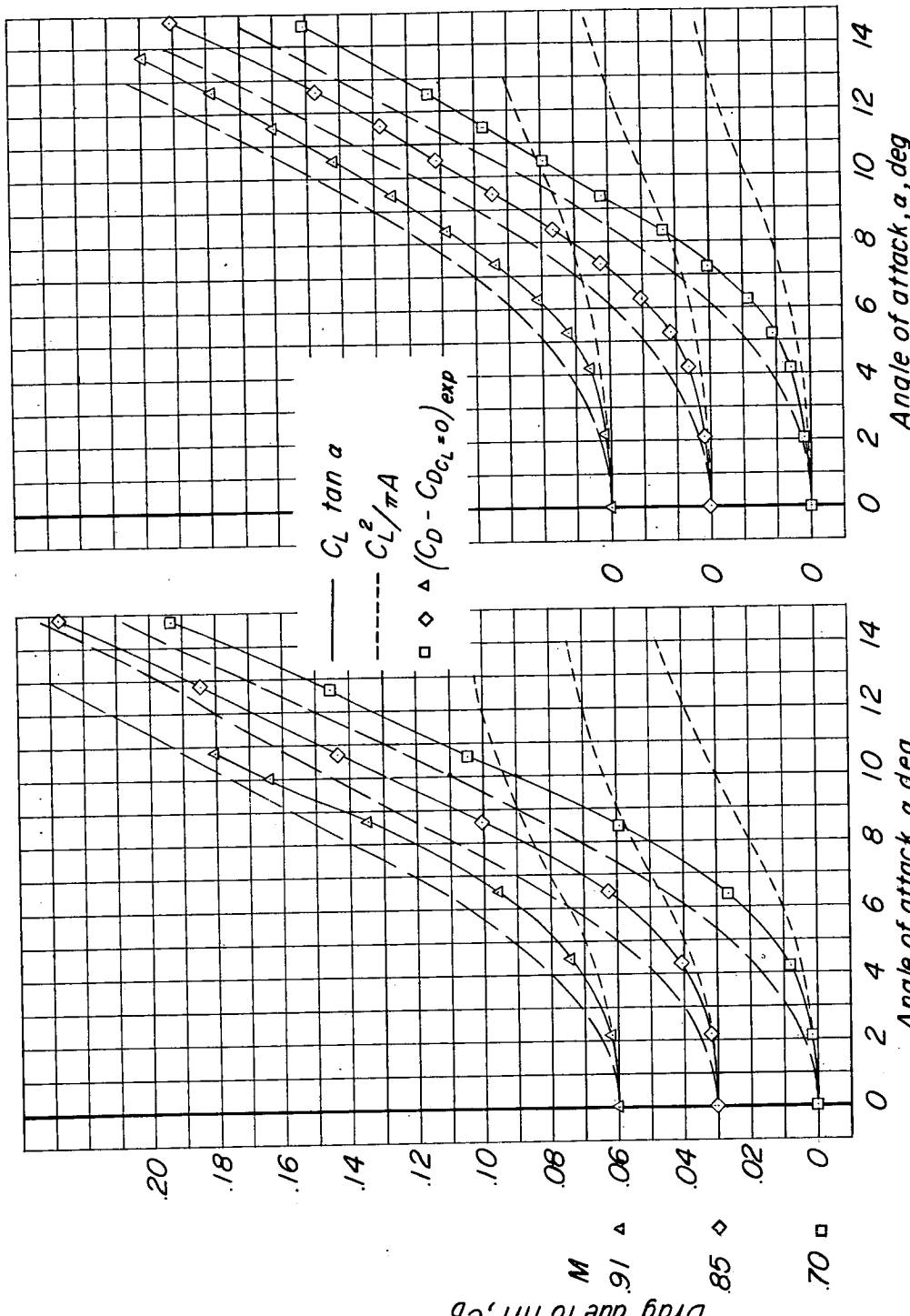

(c) 45-4-.6-006 wing.

(d) 60-4-.6-006 wing.

Figure 18.- Concluded.

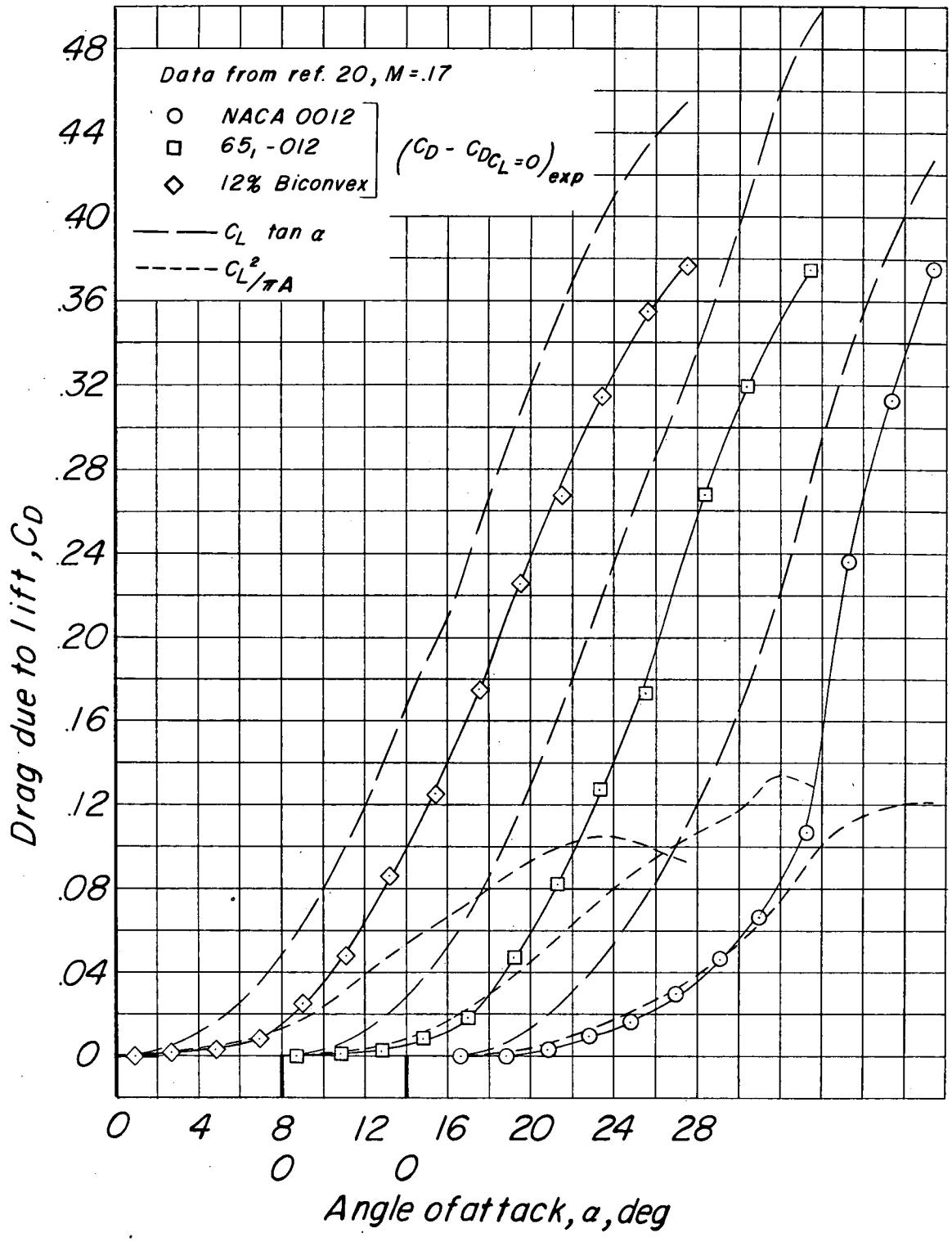

Figure 19.- Variation of low-speed drag due to lift for untapered 45° swept wings of aspect ratio 2.61.

[redacted]

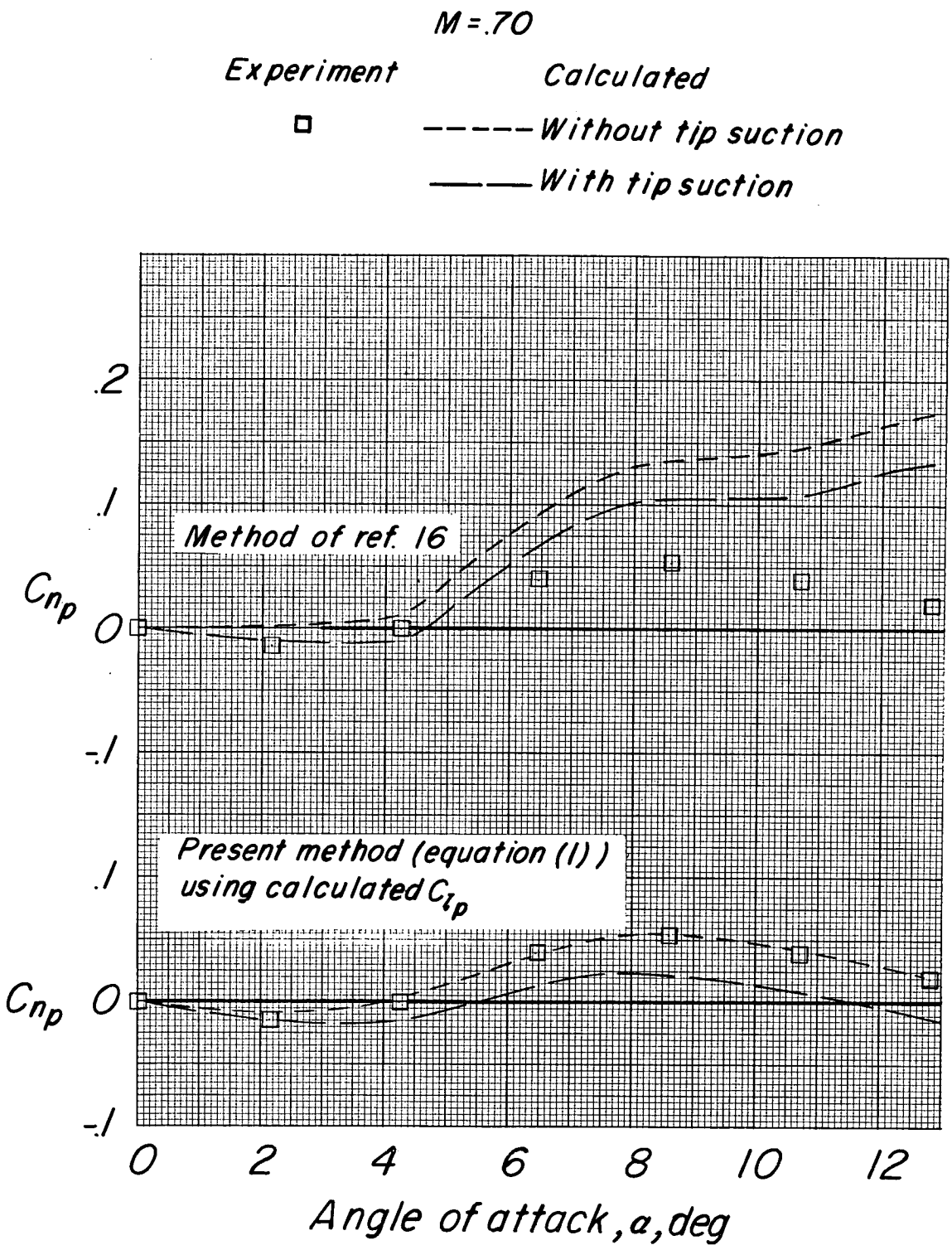

Figure 20.- Comparison of experimental values of C_{l_p} with various methods of calculation for 32.6-4-.6-006 wing.

[redacted]

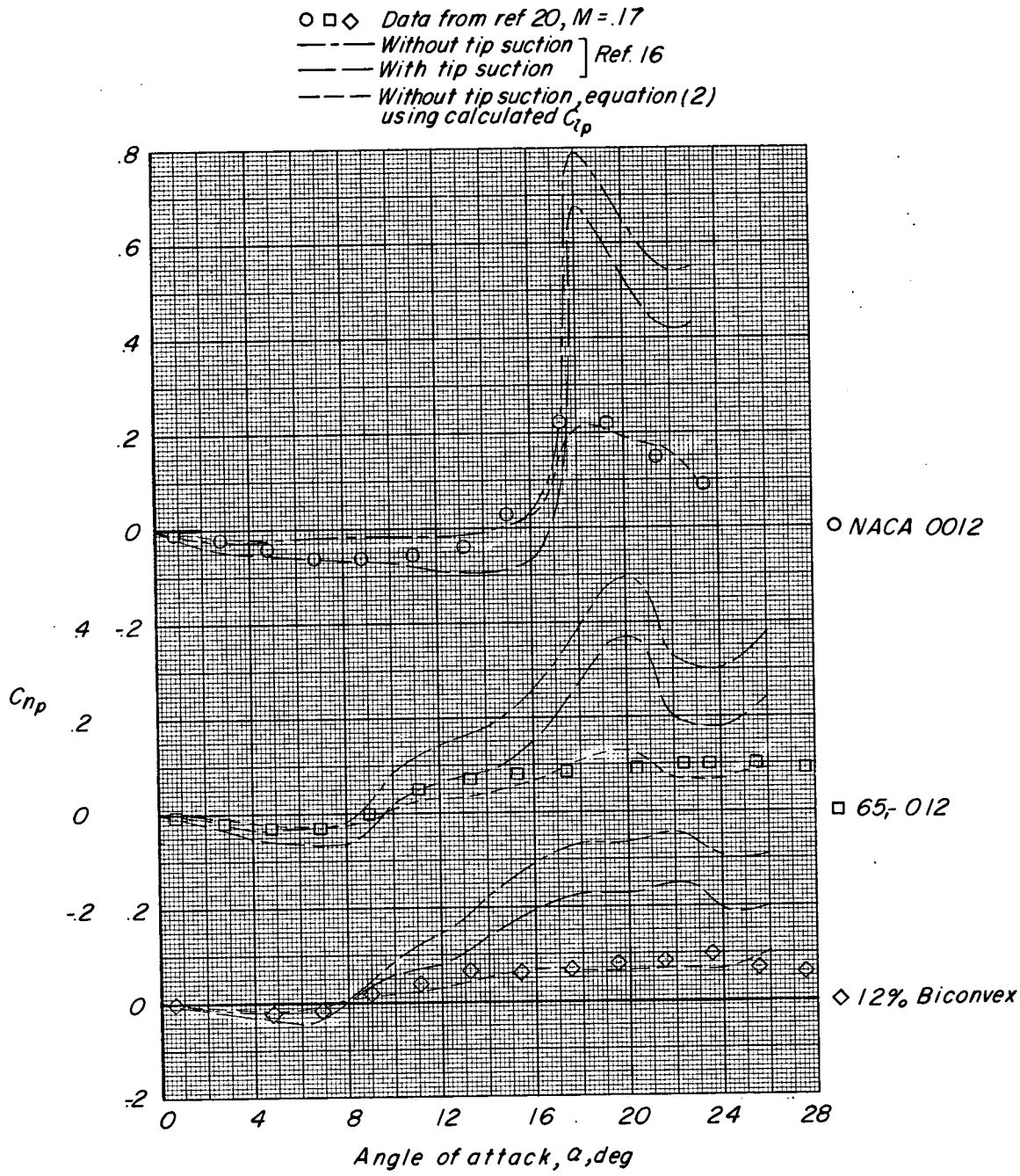

Figure 21.- Comparison of low-speed experimental C_{n_p} with calculated values for untapered 45° swept wings of aspect ratio 2.61.

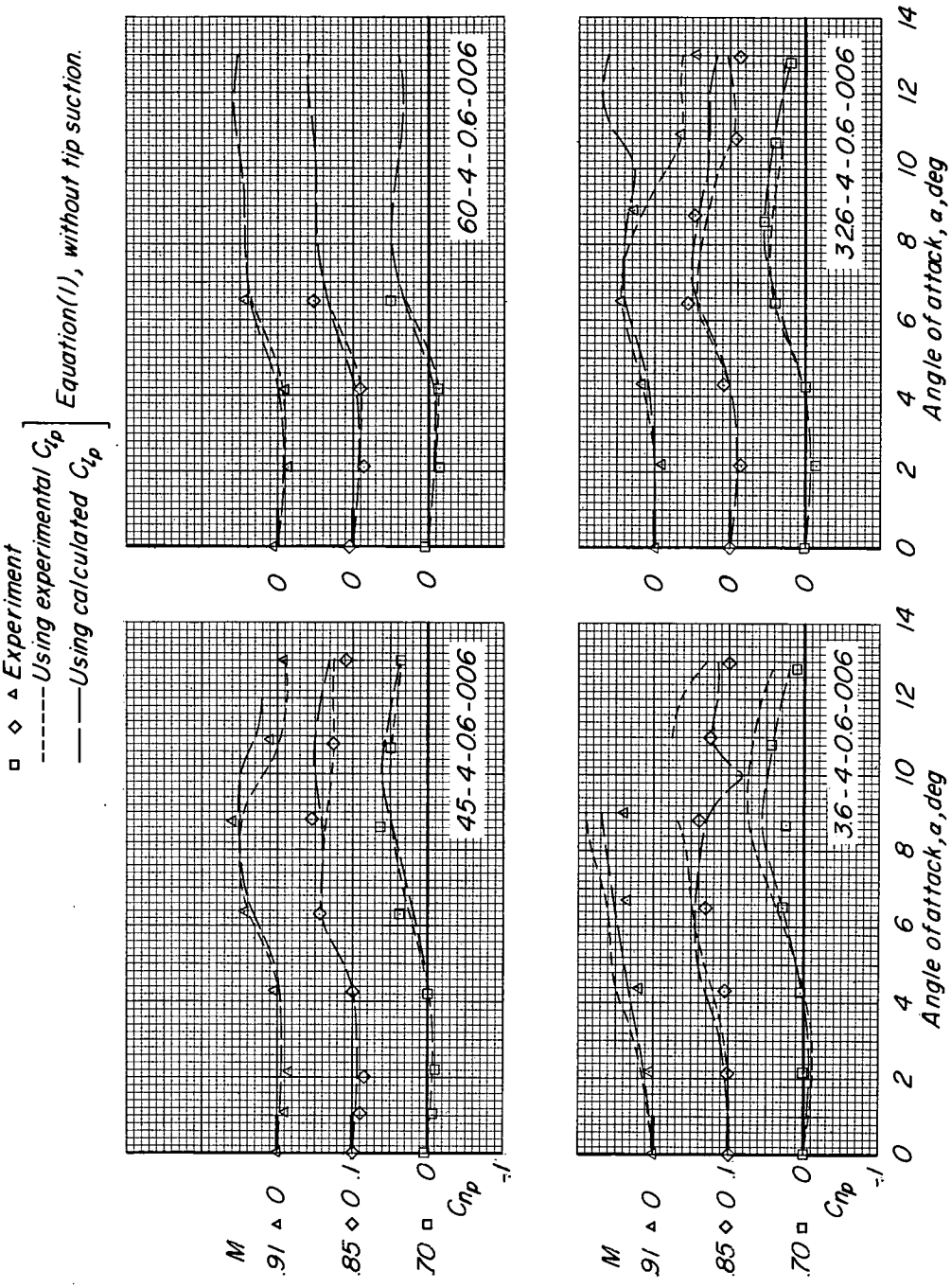

Figure 22.- Comparison of experimental and calculated variation of C_{n_p} with angle of attack.

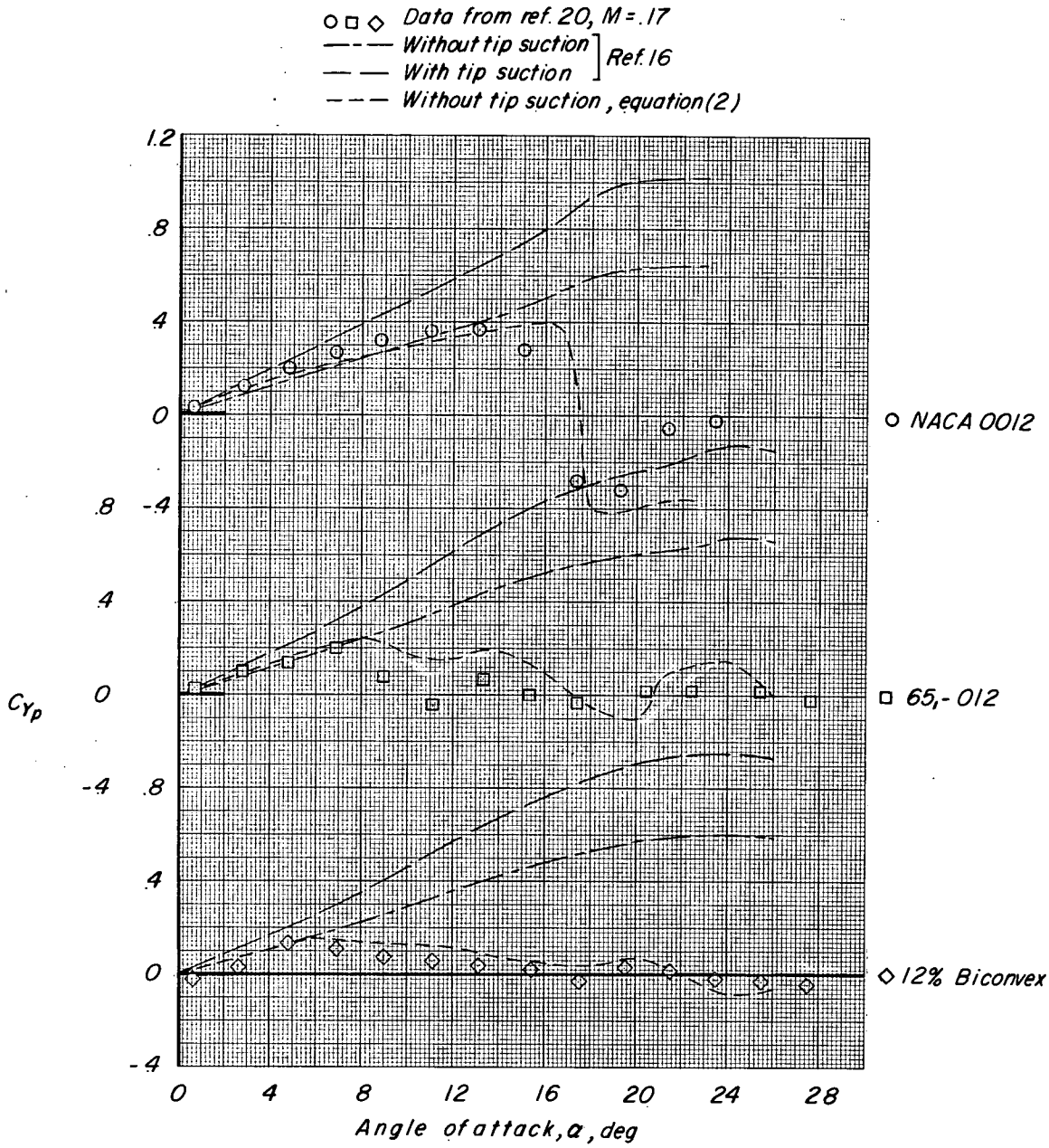

Figure 23.- Comparison of low-speed experimental C_{Y_p} with calculated values for untapered 45° swept wings of aspect ratio 2.61.

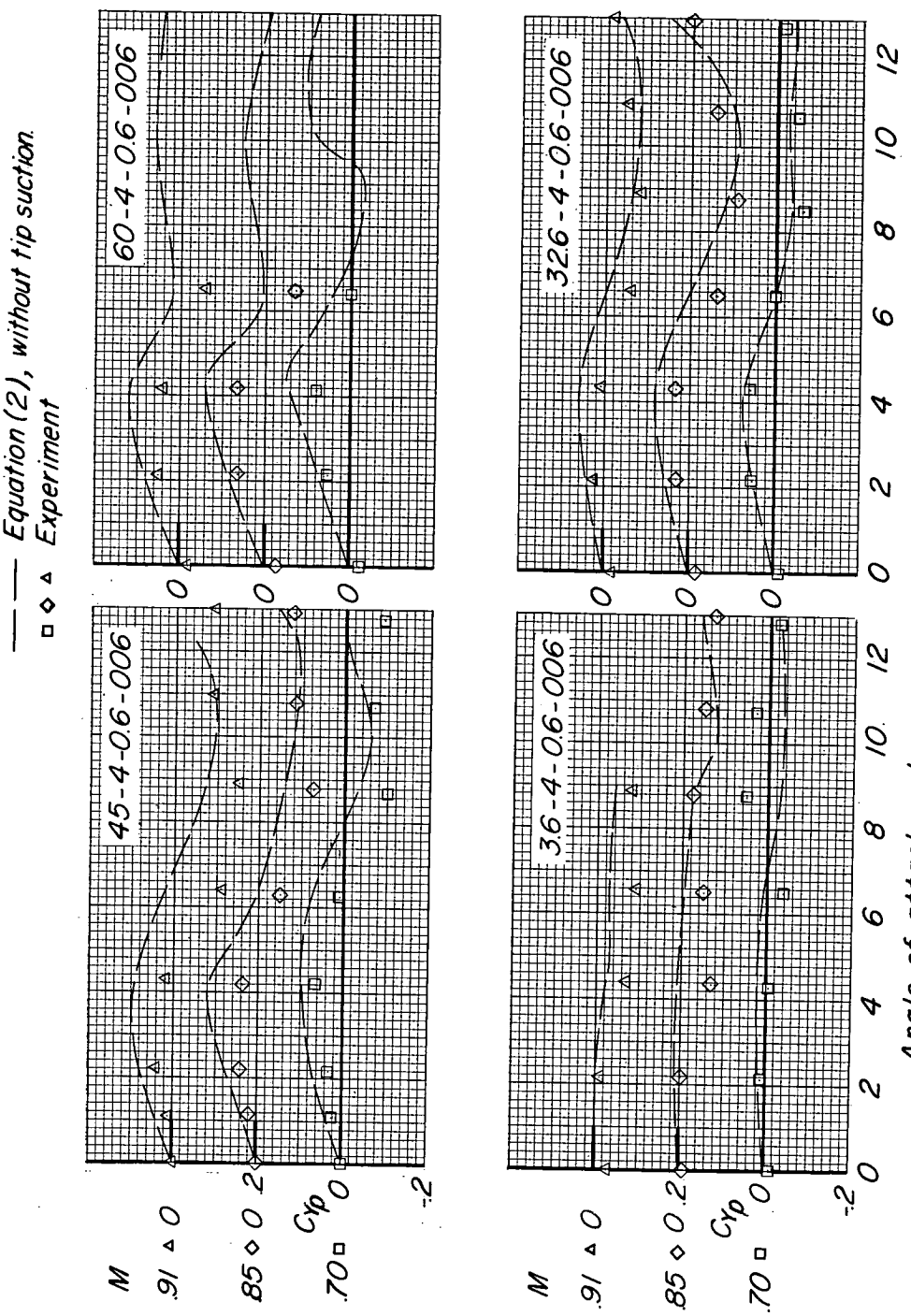

Figure 24.- Comparison of experimental and calculated variation of C_{Y_p} with angle of attack.